On the generation of surface waves in frequency selective structures

Kristensson, Gerhard

2003

CODEN:LUTEDX/(TEAT-7118)/1-38/(2003)

On the generation of surface waves in frequency selective structures

Gerhard Kristensson

Department of Electroscience
Electromagnetic Theory
Lund Institute of Technology
Sweden

Gerhard Kristensson

Department of Electroscience
Electromagnetic Theory
Lund Institute of Technology
P.O. Box 118
SE-221 00 Lund
Sweden

Editor: Gerhard Kristensson

Abstract

In this paper, we discuss and analyze the criteria for the existence and the generation of surface modes in dielectric slabs with and without metallic layers (frequency selective structures, FSS). The material parameter of the slab is in general bianisotropic, but the examples and the numerical computations show only isotropic materials. It is shown that there are three different categories of resonances occurring in power transmission and power reflection in a FSS, *i.e.*, 1) resonances in the array, 2) surface wave excitations, and 3) onset of grating lobes.

1 Introduction

Surface waves can have a devastating effect on the performance of a radome construction if such waves are excited. The purpose of this paper is to investigate the characteristics of these surface waves and how these waves are excited for radome constructions.

The concept of propagators is an analysis tool that is potent enough to analyze surface waves in general supporting materials. This technique has shown great potential [5, 10], and, moreover, the analysis is independent on any coordinate representation. Such an presentation is vital in the understanding of the more complex material situations, such as anisotropies and bianisotropies of the material.

We start by stating the prerequisites needed for the investigation in Section 2. In Section 3, we investigate surface waves in a (bianisotropic) slab without any metal screen. The slab is homogeneous w.r.t. the lateral coordinates, but can be inhomogeneous w.r.t. the depth parameter. The generation of surface waves in a slab with one metallic layer (screen) is investigated in Section 5, and its application to the periodic case (FSS) is further developed in Section 6. In Section 7 some numerical examples illustrate the results.

2 The electric and magnetic fields in the slab

We orient the coordinate system so that the normal direction to the slab is oriented parallel to the z-axis, see Figure 1. We recall the time-harmonic ($\mathrm{e}^{-i\omega t}$) constitutive relations of the general bianisotropic medium [10]:

$$\begin{cases} \boldsymbol{D} = \epsilon_0 \left\{ \boldsymbol{\epsilon} \cdot \boldsymbol{E} + \eta_0 \boldsymbol{\xi} \cdot \boldsymbol{H} \right\} \\ \boldsymbol{B} = \dfrac{1}{c_0} \left\{ \boldsymbol{\zeta} \cdot \boldsymbol{E} + \eta_0 \boldsymbol{\mu} \cdot \boldsymbol{H} \right\} \end{cases}$$

The permittivity and the permeability of vacuum are denoted by ϵ_0 and μ_0, respectively. The speed of light in vacuum is $c_0 = 1/\sqrt{\epsilon_0 \mu_0}$ and the intrinsic impedance of vacuum is $\eta_0 = \sqrt{\mu_0/\epsilon_0}$. The bianisotropic slabs may have varying material dyadics $\boldsymbol{\epsilon}$, $\boldsymbol{\xi}$, $\boldsymbol{\zeta}$, $\boldsymbol{\mu}$, as functions of depth z (and angular frequency ω), *i.e.*, $\boldsymbol{\epsilon} = \boldsymbol{\epsilon}(z)$ *etc.* The four material dyadics, $\boldsymbol{\epsilon}$, $\boldsymbol{\xi}$, $\boldsymbol{\zeta}$, $\boldsymbol{\mu}$, are dimension-less quantities. The electric and

magnetic fields, $\boldsymbol{E}$ and $\boldsymbol{H}$, respectively, and the electric and magnetic flux densities, $\boldsymbol{D}$ and $\boldsymbol{B}$, respectively, satisfy the Maxwell equations

$$\begin{cases} \nabla \times \boldsymbol{E} = ik_0 c_0 \boldsymbol{B} = ik_0 \left\{ \boldsymbol{\zeta} \cdot \boldsymbol{E} + \eta_0 \boldsymbol{\mu} \cdot \boldsymbol{H} \right\} \\ \eta_0 \nabla \times \boldsymbol{H} = -ik_0 c_0 \eta_0 \boldsymbol{D} = -ik_0 \left\{ \boldsymbol{\epsilon} \cdot \boldsymbol{E} + \eta_0 \boldsymbol{\xi} \cdot \boldsymbol{H} \right\} \end{cases}$$

where $k_0 = \omega / c_0$ is the vacuum wave number.

The electric field in any stratified material can always be represented as a Fourier transform in the lateral coordinates x and y (plane wave spectrum representation), *i.e.*, the electric field can be represented as

$$\boldsymbol{E}(\boldsymbol{k}_t, z) = \iint_{-\infty}^{\infty} \boldsymbol{E}(\boldsymbol{r}) \mathrm{e}^{-\mathrm{i}\boldsymbol{k}_t \cdot \boldsymbol{\rho}} \, \mathrm{d}x \, \mathrm{d}y$$

where

$$\boldsymbol{\rho} = \hat{\boldsymbol{x}} x + \hat{\boldsymbol{y}} y, \qquad \boldsymbol{k}_t = \hat{\boldsymbol{x}} k_x + \hat{\boldsymbol{y}} k_y$$

are the lateral position vector and lateral wave vector, respectively. By the Fourier inversion formula, the inverse Fourier transform w.r.t. $\boldsymbol{\rho}$ is

$$\boldsymbol{E}(\boldsymbol{r}) = \frac{1}{4\pi^2} \iint_{-\infty}^{\infty} \boldsymbol{E}(\boldsymbol{k}_t, z) \mathrm{e}^{\mathrm{i}\boldsymbol{k}_t \cdot \boldsymbol{\rho}} \, \mathrm{d}k_x \, \mathrm{d}k_y$$

Notice that, in order to avoid cumbersome notation, the same letter has been used to denote the Fourier transform of the field, $\boldsymbol{E}(\boldsymbol{k}_t, z)$, and the field itself, $\boldsymbol{E}(\boldsymbol{r})$, in real space. The argument of the field shows what field is intended.

The Fourier variable $\boldsymbol{k}_t$ defines two unit vectors in the x-y-plane, which constitutes the natural, coordinate-free basis for decomposing vectors and dyadics in the x-y-plane, *viz.*,

$$\hat{\boldsymbol{e}}_{\parallel} = \frac{\boldsymbol{k}_t}{k_t}, \qquad \hat{\boldsymbol{e}}_{\perp} = \mathbf{J} \cdot \hat{\boldsymbol{e}}_{\parallel} \tag{2.1}$$

where[1] $\mathbf{J} = \hat{\boldsymbol{z}} \times \mathbf{I}_3$ or $\mathbf{J} \cdot \boldsymbol{A} = \hat{\boldsymbol{z}} \times \boldsymbol{A}$, which denotes a projection of a vector $\boldsymbol{A}$ onto the x-y-plane followed by a rotation of $\pi/2$ in this plane. The non-negative number

$$k_t = \sqrt{k_x^2 + k_y^2} \geq 0$$

is the lateral wave number. Notice that $\mathbf{J} \cdot \mathbf{J} = -\mathbf{I}_2$. Moreover, the normal (longitudinal) wave number, k_z, is defined by

$$k_z = \left(k_0^2 - k_t^2 \right)^{1/2} = \begin{cases} \sqrt{k_0^2 - k_t^2} \text{ for } k_t < k_0 \\ \mathrm{i}\sqrt{k_t^2 - k_0^2} \text{ for } k_t > k_0 \end{cases}$$

[1]Note the typographical difference between the dyadic $\mathbf{J}$ which denotes a rotation, and the current density vector $\boldsymbol{J}$. All vectors in this paper are typed in italic bold face and dyadics are typed in roman bold face. The identity dyadic in n dimensions is denoted $\mathbf{I}_n$.

where the standard convention of the square root of a positive argument is intended. With these unit vectors, $\hat{\boldsymbol{e}}_\parallel$ and $\hat{\boldsymbol{e}}_\perp$, the two classical classification categories of TM- and TE-waves in an isotropic material correspond to the polarization vectors of the electric field along

$$\begin{cases} \hat{\boldsymbol{e}}_\parallel, \text{ TM-case} \\ \hat{\boldsymbol{e}}_\perp, \text{ TE-case} \end{cases}$$

respectively.

2.1 Fundamental equation

All vector fields are decomposed into their transverse x-y-components and their z-components, *e.g.*,

$$\begin{cases} \boldsymbol{E}(\boldsymbol{r}) = \boldsymbol{E}_{xy}(\boldsymbol{r}) + \hat{\boldsymbol{z}} E_z(\boldsymbol{r}) \\ \boldsymbol{E}(\boldsymbol{k}_t, z) = \boldsymbol{E}_{xy}(\boldsymbol{k}_t, z) + \hat{\boldsymbol{z}} E_z(\boldsymbol{k}_t, z) \end{cases}$$

The transverse components satisfy the fundamental equation [10], *i.e.*,

$$\frac{\mathrm{d}}{\mathrm{d}z} \begin{pmatrix} \boldsymbol{E}_{xy}(\boldsymbol{k}_t, z) \\ \eta_0 \mathbf{J} \cdot \boldsymbol{H}_{xy}(\boldsymbol{k}_t, z) \end{pmatrix} = ik_0 \mathbf{M}(\boldsymbol{k}_t, z) \cdot \begin{pmatrix} \boldsymbol{E}_{xy}(\boldsymbol{k}_t, z) \\ \eta_0 \mathbf{J} \cdot \boldsymbol{H}_{xy}(\boldsymbol{k}_t, z) \end{pmatrix} \tag{2.2}$$

where the linear map $\mathbf{M}(\boldsymbol{k}_t, z)\colon \mathbb{C}^{2\times 2} \to \mathbb{C}^{2\times 2}$ depends on the material dyadics. A detailed representation of $\mathbf{M}(\boldsymbol{k}_t, z)$ in terms of $\boldsymbol{\epsilon}(z)$, $\boldsymbol{\xi}(z)$, $\boldsymbol{\zeta}(z)$, $\boldsymbol{\mu}(z)$, $\boldsymbol{k}_t$, and k_0 is given in [10].

In this paper, we adopt the notion of a decomposition of a four-dimensional dyadic, *e.g.*, $\mathbf{M}$, into a matrix of two-dimensional dyadics, $\mathbf{M}_{ij}$, $i, j = 1, 2$ as

$$\mathbf{M} = \begin{pmatrix} \mathbf{M}_{11} & \mathbf{M}_{12} \\ \mathbf{M}_{21} & \mathbf{M}_{22} \end{pmatrix}$$

From the transverse field components of the electric and the magnetic field in the spectral domain, $\boldsymbol{E}_{xy}(\boldsymbol{k}_t, z)$ and $\boldsymbol{H}_{xy}(\boldsymbol{k}_t, z)$, all other field components can be determined. Specifically, the z-components of the electric and the magnetic fields are given terms of their transverse components as [10]

$$\begin{aligned} &\begin{pmatrix} \epsilon_{zz}(z) & \xi_{zz}(z) \\ \zeta_{zz}(z) & \mu_{zz}(z) \end{pmatrix} \begin{pmatrix} E_z(z) \\ \eta_0 H_z(z) \end{pmatrix} \\ &\quad = \begin{pmatrix} -\boldsymbol{\epsilon}_z(z) & \boldsymbol{k}_t/k_0 + \boldsymbol{\xi}_z(z) \cdot \mathbf{J} \\ \mathbf{J} \cdot \boldsymbol{k}_t/k_0 - \boldsymbol{\zeta}_z(z) & \boldsymbol{\mu}_z(z) \cdot \mathbf{J} \end{pmatrix} \cdot \begin{pmatrix} \boldsymbol{E}_{xy}(z) \\ \eta_0 \mathbf{J} \cdot \boldsymbol{H}_{xy}(z) \end{pmatrix} \end{aligned} \tag{2.3}$$

2.2 Propagators

The concept of propagators is of fundamental importance for the systematic analysis presented in this paper. The propagators have been introduced in *e.g.*, [9, 10].

Let $z_0 < z < z_1$. The propagator of the transverse electric and magnetic fields is [9, 10]

$$\begin{pmatrix} \boldsymbol{E}_{xy}(\boldsymbol{k}_t, z) \\ \eta_0 \mathbf{J} \cdot \boldsymbol{H}_{xy}(\boldsymbol{k}_t, z) \end{pmatrix} = \mathbf{P}(\boldsymbol{k}_t, z, z_0) \cdot \begin{pmatrix} \boldsymbol{E}_{xy}(\boldsymbol{k}_t, z_0) \\ \eta_0 \mathbf{J} \cdot \boldsymbol{H}_{xy}(\boldsymbol{k}_t, z_0) \end{pmatrix} \tag{2.4}$$

or in a decomposition of the four-dimensional dyadic $\mathbf{P}$ in four two-dimensional dyadics as described above, we get

$$\begin{cases} \boldsymbol{E}_{xy}(\boldsymbol{k}_t, z) = \mathbf{P}_{11}(\boldsymbol{k}_t, z, z_0) \cdot \boldsymbol{E}_{xy}(\boldsymbol{k}_t, z_0) + \mathbf{P}_{12}(\boldsymbol{k}_t, z, z_0) \cdot \eta_0 \mathbf{J} \cdot \boldsymbol{H}_{xy}(\boldsymbol{k}_t, z_0) \\ \eta_0 \mathbf{J} \cdot \boldsymbol{H}_{xy}(\boldsymbol{k}_t, z) = \mathbf{P}_{21}(\boldsymbol{k}_t, z, z_0) \cdot \boldsymbol{E}_{xy}(\boldsymbol{k}_t, z_0) + \mathbf{P}_{22}(\boldsymbol{k}_t, z, z_0) \cdot \eta_0 \mathbf{J} \cdot \boldsymbol{H}_{xy}(\boldsymbol{k}_t, z_0) \end{cases}$$

For $z = z_0$ the propagators are the identity transformation in four dimensions, $\mathbf{I}_4$. The propagator $\mathbf{P}$ satisfy a system of ordinary differential equations (ODE). They are [9, 10]

$$\begin{cases} \dfrac{\mathrm{d}}{\mathrm{d}z}\mathbf{P}(\boldsymbol{k}_t, z, z_0) = \mathrm{i}k_0 \mathbf{M}(\boldsymbol{k}_t, z) \cdot \mathbf{P}(\boldsymbol{k}_t, z, z_0) \\ \mathbf{P}(z_0, z_0) = \mathbf{I}_4 \end{cases} \tag{2.5}$$

where the dyadic $\mathbf{M}$ is the same as in (2.2).

These equations relate the fields at one position, z_0, to the fields at another position, z. In this way, they propagate the fields from one position to another. The propagation from z_0 to z can be made in one single step or in several small ones. This property imply that the propagators show group properties in the depth variable, *i.e.*,

$$\mathbf{P}(z_2, z_0) = \mathbf{P}(z_2, z_1) \cdot \mathbf{P}(z_1, z_0) \tag{2.6}$$

Since it can be proved that the dyadic $\mathbf{P}(\boldsymbol{k}_t, z, z_0)$ is an entire dyadic-valued function of $\boldsymbol{k}_t$, the singularities of $\boldsymbol{E}_{xy}(\boldsymbol{k}_t, z)$ are the same as $\boldsymbol{E}_{xy}(\boldsymbol{k}_t, z_0)$ and $\boldsymbol{H}_{xy}(\boldsymbol{k}_t, z_0)$.

2.3 Wave splitting

The fields inside the slab are most conveniently represented as the total transverse electric and magnetic fields and not as the right- and left-going components of the field. However, outside the slab, we like to identify the input and output fields of the slab. The input fields are commonly called the incident fields and the output fields are the reflected and transmitted fields. To find these fields, we decompose the total fields—the wave splitting transformation.

Wave splitting gives [9, 10]

$$\begin{pmatrix} \boldsymbol{E}_{xy}(\boldsymbol{k}_t, z) \\ \eta_0 \mathbf{J} \cdot \boldsymbol{H}_{xy}(\boldsymbol{k}_t, z) \end{pmatrix} = \begin{pmatrix} \mathbf{I}_2 & \mathbf{I}_2 \\ -\mathbf{W}^{-1}(\boldsymbol{k}_t) & \mathbf{W}^{-1}(\boldsymbol{k}_t) \end{pmatrix} \cdot \begin{pmatrix} \boldsymbol{F}^+(\boldsymbol{k}_t, z) \\ \boldsymbol{F}^-(\boldsymbol{k}_t, z) \end{pmatrix} \tag{2.7}$$

where the two-dimensional dyadic $\mathbf{W}^{-1}$ is the vacuum wave splitting dyadic

$$\mathbf{W}^{-1}(\boldsymbol{k}_t) = \hat{\boldsymbol{e}}_{\parallel}\hat{\boldsymbol{e}}_{\parallel}\frac{k_0}{k_z} + \hat{\boldsymbol{e}}_{\perp}\hat{\boldsymbol{e}}_{\perp}\frac{k_z}{k_0} \tag{2.8}$$

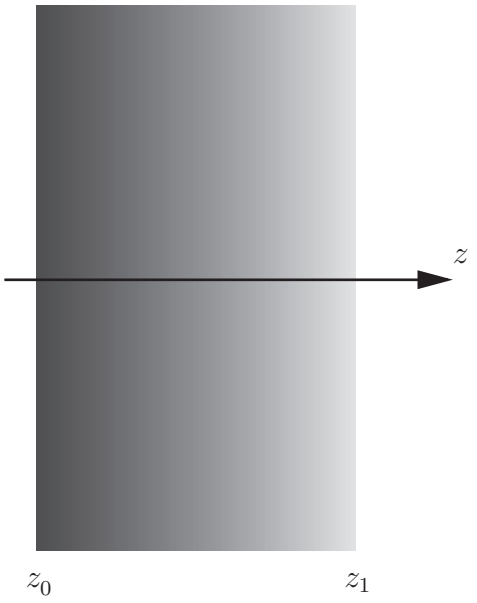

Figure 1: The geometry of the slab without screens.

Here, $\mathbf{I}_2$ is the identity dyadic in the x-y-plane, and $\hat{\boldsymbol{e}}_\parallel(\boldsymbol{k}_t)$ and $\hat{\boldsymbol{e}}_\perp(\boldsymbol{k}_t)$, defined in (2.1), constitute a orthogonal basis for the lateral vectors (vectors in the x-y-plane). The inverse of the vacuum wave splitting dyadic is

$$\mathbf{W}(\boldsymbol{k}_t) = \hat{\boldsymbol{e}}_\parallel \hat{\boldsymbol{e}}_\parallel \frac{k_z}{k_0} + \hat{\boldsymbol{e}}_\perp \hat{\boldsymbol{e}}_\perp \frac{k_0}{k_z} \tag{2.9}$$

We also have the inverse of (2.7) [9, 10]

$$\begin{pmatrix} \boldsymbol{F}^+(\boldsymbol{k}_t, z) \\ \boldsymbol{F}^-(\boldsymbol{k}_t, z) \end{pmatrix} = \frac{1}{2} \begin{pmatrix} \mathbf{I}_2 & -\mathbf{W}(\boldsymbol{k}_t) \\ \mathbf{I}_2 & \mathbf{W}(\boldsymbol{k}_t) \end{pmatrix} \cdot \begin{pmatrix} \boldsymbol{E}_{xy}(\boldsymbol{k}_t, z) \\ \eta_0 \mathbf{J} \cdot \boldsymbol{H}_{xy}(\boldsymbol{k}_t, z) \end{pmatrix} \tag{2.10}$$

It is pertinent to introduce the following two four-dimensional dyadics $\mathbf{S}$ and $\mathbf{S}^{-1}$ defined by

$$\mathbf{S}(\boldsymbol{k}_t) = \frac{1}{2} \begin{pmatrix} \mathbf{I}_2 & -\mathbf{W}(\boldsymbol{k}_t) \\ \mathbf{I}_2 & \mathbf{W}(\boldsymbol{k}_t) \end{pmatrix}, \qquad \mathbf{S}^{-1}(\boldsymbol{k}_t) = \begin{pmatrix} \mathbf{I}_2 & \mathbf{I}_2 \\ -\mathbf{W}^{-1}(\boldsymbol{k}_t) & \mathbf{W}^{-1}(\boldsymbol{k}_t) \end{pmatrix}$$

These dyadics are used frequently in the analysis below.

3 Bianisotropic slab without metallic screens

We start the analysis of surface waves by considering a bianisotropic slab, which can be inhomogeneous w.r.t. the depth parameter z, see Figure 1. The end points of the slab are denoted $z = z_0$ and $z = z_1$, respectively.

From (2.4) and (2.7) we get (below, we often, for convenience, omit the dependence of the transverse wave vector $\boldsymbol{k}_t$)

$$\begin{pmatrix} \boldsymbol{E}_{xy}(z_1) \\ \eta_0 \mathbf{J} \cdot \boldsymbol{H}_{xy}(z_1) \end{pmatrix} = \mathbf{P}(z_1, z_0) \cdot \begin{pmatrix} \boldsymbol{E}_{xy}(z_0) \\ \eta_0 \mathbf{J} \cdot \boldsymbol{H}_{xy}(z_0) \end{pmatrix} = \mathbf{P}(z_1, z_0) \cdot \mathbf{S}^{-1} \cdot \begin{pmatrix} \boldsymbol{F}^+(z_0) \\ \boldsymbol{F}^-(z_0) \end{pmatrix}$$

Moreover, from (2.10)

$$\begin{aligned} \begin{pmatrix} \boldsymbol{F}^+(z_1) \\ \boldsymbol{F}^-(z_1) \end{pmatrix} =& \mathbf{S} \cdot \begin{pmatrix} \boldsymbol{E}_{xy}(z_1) \\ \eta_0 \mathbf{J} \cdot \boldsymbol{H}_{xy}(z_1) \end{pmatrix} = \mathbf{S} \cdot \mathbf{P}(z_1, z_0) \cdot \mathbf{S}^{-1} \cdot \begin{pmatrix} \boldsymbol{F}^+(z_0) \\ \boldsymbol{F}^-(z_0) \end{pmatrix} \\ =& \mathbf{G}(z_1, z_0) \cdot \mathbf{S}^{-1} \cdot \begin{pmatrix} \boldsymbol{F}^+(z_0) \\ \boldsymbol{F}^-(z_0) \end{pmatrix} = \mathbf{T}(z_1, z_0) \cdot \begin{pmatrix} \boldsymbol{F}^+(z_0) \\ \boldsymbol{F}^-(z_0) \end{pmatrix} \end{aligned} \tag{3.1}$$

where

$$\mathbf{G}(z_1, z_0) = \mathbf{S} \cdot \mathbf{P}(z_1, z_0), \quad \text{or} \quad \begin{cases} 2\mathbf{G}_{11} = \mathbf{P}_{11} - \mathbf{W} \cdot \mathbf{P}_{21} \\ 2\mathbf{G}_{12} = \mathbf{P}_{12} - \mathbf{W} \cdot \mathbf{P}_{22} \\ 2\mathbf{G}_{21} = \mathbf{P}_{11} + \mathbf{W} \cdot \mathbf{P}_{21} \\ 2\mathbf{G}_{22} = \mathbf{P}_{12} + \mathbf{W} \cdot \mathbf{P}_{22} \end{cases} \tag{3.2}$$

and

$$\mathbf{T}(z_1, z_0) = \mathbf{G}(z_1, z_0) \cdot \mathbf{S}^{-1}, \quad \text{or} \quad \begin{cases} \mathbf{T}_{11} = \mathbf{G}_{11} - \mathbf{G}_{12} \cdot \mathbf{W}^{-1} \\ \mathbf{T}_{12} = \mathbf{G}_{11} + \mathbf{G}_{12} \cdot \mathbf{W}^{-1} \\ \mathbf{T}_{21} = \mathbf{G}_{21} - \mathbf{G}_{22} \cdot \mathbf{W}^{-1} \\ \mathbf{T}_{22} = \mathbf{G}_{21} + \mathbf{G}_{22} \cdot \mathbf{W}^{-1} \end{cases} \tag{3.3}$$

Especially, since $\mathbf{P}(z_0, z_0) = \mathbf{I}_4$

$$\mathbf{T}(z_0, z_0) = \mathbf{I}_4$$

The dyadics $\mathbf{G}_{ij}$ and $\mathbf{T}_{ij}$, $i, j = 1, 2$, are all analytic, dyadic-valued functions of $\boldsymbol{k}_t$, except for a branch point (or pole) at $\boldsymbol{k}_t = k_0 \hat{\boldsymbol{e}}_\parallel$.

3.1 The properties of the dyadics G and T

The group properties, (2.6), of the the propagators $\mathbf{P}$ imply

$$\mathbf{G}(z_1, z_0) = \mathbf{G}(z_1, z) \cdot \mathbf{P}(z, z_0) \tag{3.4}$$

and, since $\mathbf{P}^{-1}(z_1, z_0) = \mathbf{P}(z_0, z_1)$

$$(\mathbf{G}(z_1, z_0))^{-1} = \mathbf{P}(z_0, z_1) \cdot \mathbf{S}^{-1} = \mathbf{S}^{-1} \cdot \mathbf{T}(z_0, z_1)$$

Moreover, we have, due to the group properties, (2.6), of the the propagators $\mathbf{P}$

$$\mathbf{T}(z_2, z_1) \cdot \mathbf{T}(z_1, z_0) = \mathbf{S} \cdot \mathbf{P}(z_2, z_1) \cdot \mathbf{S}^{-1} \cdot \mathbf{S} \cdot \mathbf{P}(z_1, z_0) \cdot \mathbf{S}^{-1} = \mathbf{T}(z_2, z_0)$$

Especially, since $\mathbf{T}(z_1, z_1) = \mathbf{I}_4$

$$\mathbf{T}(z_1, z_0) \cdot \mathbf{T}(z_0, z_1) = \mathbf{I}_4$$

and

$$\mathbf{T}(z_1, z_0) \cdot \mathbf{G}(z_0, z) = \mathbf{G}(z_1, z_0) \cdot \mathbf{P}(z_0, z) = \mathbf{G}(z_1, z)$$

This latter equation implies

$$\mathbf{T}(z_2, z_0) = \mathbf{G}(z_2, z_1) \cdot (\mathbf{G}(z_0, z_1))^{-1} \tag{3.5}$$

3.2 Scattering representation

Equation (3.1) gives the relation between the split fields at both ends of the slab, *i.e.*, at $z = z_0$ and $z = z_1$. A more common representation (scattering representation) is to relate $\boldsymbol{F}^-(z_0)$ and $\boldsymbol{F}^+(z_1)$ (output fields) in terms of $\boldsymbol{F}^+(z_0)$ and $\boldsymbol{F}^-(z_1)$ (input fields). Since, from (3.1)

$$\boldsymbol{F}^-(z_0) = \mathbf{T}_{22}^{-1} \cdot \boldsymbol{F}^-(z_1) - \mathbf{T}_{22}^{-1} \cdot \mathbf{T}_{21} \cdot \boldsymbol{F}^+(z_0) \tag{3.6}$$

we get

$$\boldsymbol{F}^+(z_1) = \mathbf{T}_{11} \cdot \boldsymbol{F}^+(z_0) + \mathbf{T}_{12} \cdot \left(\mathbf{T}_{22}^{-1} \cdot \boldsymbol{F}^-(z_1) - \mathbf{T}_{22}^{-1} \cdot \mathbf{T}_{21} \cdot \boldsymbol{F}^+(z_0)\right)$$

or in a matrix form

$$\begin{pmatrix} \boldsymbol{F}^-(z_0) \\ \boldsymbol{F}^+(z_1) \end{pmatrix} = \begin{pmatrix} -\mathbf{T}_{22}^{-1} \cdot \mathbf{T}_{21} & \mathbf{T}_{22}^{-1} \\ \mathbf{T}_{11} - \mathbf{T}_{12} \cdot \mathbf{T}_{22}^{-1} \cdot \mathbf{T}_{21} & \mathbf{T}_{12} \cdot \mathbf{T}_{22}^{-1} \end{pmatrix} \cdot \begin{pmatrix} \boldsymbol{F}^+(z_0) \\ \boldsymbol{F}^-(z_1) \end{pmatrix}$$

The arguments of all dyadics $\mathbf{T}_{ij}$ here are $\mathbf{T}_{ij} = \mathbf{T}_{ij}(z_1, z_0)$, $i, j = 1, 2$.

This is the desired relation between the output fields, $\boldsymbol{F}^-(z_0)$ and $\boldsymbol{F}^+(z_1)$, and the input fields, $\boldsymbol{F}^+(z_0)$ and $\boldsymbol{F}^-(z_1)$ for a slab without any metallic screens.

3.3 Surface waves characterization—the internal fields

We proceed in our quest for a coordinate independent representation of the fields in the slab. The surface waves are defined by the $\boldsymbol{k}_t$-values at which the electric field (or magnetic field) is singular.

To find the $\boldsymbol{k}_t$-values at which the electric field is singular, we like to express the transverse electric and magnetic fields inside the slab in terms of the excitations $\boldsymbol{F}^+(\boldsymbol{k}_t, z_0)$ and $\boldsymbol{F}^-(\boldsymbol{k}_t, z_1)$, *i.e.*,

$$\begin{pmatrix} \boldsymbol{E}_{xy}(\boldsymbol{k}_t, z_0) \\ \eta_0 \mathbf{J} \cdot \boldsymbol{H}_{xy}(\boldsymbol{k}_t, z_0) \end{pmatrix} = \begin{pmatrix} \mathbf{A}(\boldsymbol{k}_t) & \mathbf{B}(\boldsymbol{k}_t) \\ \mathbf{C}(\boldsymbol{k}_t) & \mathbf{D}(\boldsymbol{k}_t) \end{pmatrix} \cdot \begin{pmatrix} \boldsymbol{F}^+(\boldsymbol{k}_t, z_0) \\ \boldsymbol{F}^-(\boldsymbol{k}_t, z_1) \end{pmatrix} \tag{3.7}$$

from which we conclude that the singular values of the fields originate from the singular $\boldsymbol{k}_t$-values of the dyadics $\mathbf{A}(\boldsymbol{k}_t)$, $\mathbf{B}(\boldsymbol{k}_t)$, $\mathbf{C}(\boldsymbol{k}_t)$, and $\mathbf{D}(\boldsymbol{k}_t)$.

From equation (3.6) we get

$$\begin{pmatrix} \boldsymbol{F}^+(z_0) \\ \boldsymbol{F}^-(z_0) \end{pmatrix} = \begin{pmatrix} \mathbf{I}_2 & \mathbf{0} \\ -\mathbf{T}_{22}^{-1} \cdot \mathbf{T}_{21} & \mathbf{T}_{22}^{-1} \end{pmatrix} \cdot \begin{pmatrix} \boldsymbol{F}^+(z_0) \\ \boldsymbol{F}^-(z_1) \end{pmatrix}$$

Finally, we get by (2.7)

$$\begin{pmatrix} \mathbf{A} & \mathbf{B} \\ \mathbf{C} & \mathbf{D} \end{pmatrix} = \begin{pmatrix} \mathbf{I}_2 & \mathbf{I}_2 \\ -\mathbf{W}^{-1} & \mathbf{W}^{-1} \end{pmatrix} \cdot \begin{pmatrix} \mathbf{I}_2 & \mathbf{0} \\ -\mathbf{T}_{22}^{-1} \cdot \mathbf{T}_{21} & \mathbf{T}_{22}^{-1} \end{pmatrix}$$

or

$$\begin{cases} \mathbf{A} = \mathbf{I}_2 - \mathbf{T}_{22}^{-1} \cdot \mathbf{T}_{21} = 2\mathbf{T}_{22}^{-1} \cdot \mathbf{G}_{22} \cdot \mathbf{W}^{-1} \\ \mathbf{B} = \mathbf{T}_{22}^{-1} \\ \mathbf{C} = -\mathbf{W}^{-1} \cdot \left(\mathbf{I}_2 + \mathbf{T}_{22}^{-1} \cdot \mathbf{T}_{21}\right) = -2\mathbf{W}^{-1} \cdot \mathbf{T}_{22}^{-1} \cdot \mathbf{G}_{21} \\ \mathbf{D} = \mathbf{W}^{-1} \cdot \mathbf{T}_{22}^{-1} \end{cases} \tag{3.8}$$

The arguments of all dyadics $\mathbf{T}_{ij}$ and $\mathbf{G}_{ij}$ here are $\mathbf{T}_{ij} = \mathbf{T}_{ij}(z_1, z_0)$ and $\mathbf{G}_{ij} = \mathbf{G}_{ij}(z_1, z_0)$, $i, j = 1, 2$.

The singularities are determined by the existence of a zero eigenvalue of the following dyadic, *cf.* also [9]: ($\boldsymbol{k}_t = k_0 \hat{\boldsymbol{e}}_\parallel$ is a branch point)

$$\mathbf{T}_{22} = \mathbf{G}_{21} + \mathbf{G}_{22} \cdot \mathbf{W}^{-1} = \frac{1}{2} \left(\mathbf{P}_{11} + \mathbf{W} \cdot \mathbf{P}_{21} + (\mathbf{P}_{12} + \mathbf{W} \cdot \mathbf{P}_{22}) \cdot \mathbf{W}^{-1} \right)$$

where all propagators have the argument (z_1, z_0). For each fixed direction in Fourier $\boldsymbol{k}_t$-space ($\hat{\boldsymbol{k}}_{\boldsymbol{t}}$ fixed), we assume that $\boldsymbol{k}_t$ is singular at $|\boldsymbol{k}_t| = k_{t\mathrm{sw}}(\hat{\boldsymbol{k}}_{\boldsymbol{t}})$. We denote these singular vectors by $\boldsymbol{k}_{t\mathrm{sw}}(\hat{\boldsymbol{k}}_{\boldsymbol{t}})$. We assume these singular values are discrete in the radial direction ($\hat{\boldsymbol{k}}_{\boldsymbol{t}}$ fixed) and finite in number for each value of the wave number k_0.

Note that for a grounded slab the surface waves are determined by the zero eigenvalues and eigenvectors of [6]

$$\mathbf{W}^{-1} \cdot \mathbf{P}_{12}(d, 0) + \mathbf{P}_{22}(d, 0) = 2\mathbf{W}^{-1} \cdot \mathbf{G}_{22}(d, 0)$$

3.4 The surface wave field

The form of the surface field is determined by the singular part of the field representation in the spatial representation (3.7). The general expression for the field is given by the inverse Fourier transform.

$$\boldsymbol{E}_{xy}(\boldsymbol{r}) = \frac{1}{4\pi^2} \iint_{-\infty}^{\infty} \mathbf{T}_{22}^{-1} \cdot \left\{ (\mathbf{T}_{22} - \mathbf{T}_{21}) \cdot \boldsymbol{F}^+(\boldsymbol{k}_t, z_0) + \boldsymbol{F}^-(\boldsymbol{k}_t, z_1) \right\} \mathrm{e}^{\mathrm{i}\boldsymbol{k}_t \cdot \boldsymbol{\rho}} \, \mathrm{d}k_x \, \mathrm{d}k_y$$

where we have used (3.7) and (3.8). This implies that the electric and the magnetic parts of the surface fields are

$$\begin{cases} \boldsymbol{E}_{xy_{\mathrm{sw}}}(\boldsymbol{\rho}, z_0) = \dfrac{\mathrm{i}}{2\pi} \displaystyle\int_0^{2\pi} \mathbf{A}_{-1}(k_{t\mathrm{sw}}(\hat{\boldsymbol{k}}_{\boldsymbol{t}})) \\ \qquad \cdot \left\{ \boldsymbol{F}^-(\boldsymbol{k}_{t\mathrm{sw}}(\hat{\boldsymbol{k}}_{\boldsymbol{t}}), z_1) - \mathbf{T}_{21}(\boldsymbol{k}_{t\mathrm{sw}}(\hat{\boldsymbol{k}}_{\boldsymbol{t}})) \cdot \boldsymbol{F}^+(\boldsymbol{k}_{t\mathrm{sw}}(\hat{\boldsymbol{k}}_{\boldsymbol{t}}), z_0) \right\} \mathrm{e}^{\mathrm{i}\boldsymbol{k}_{t\mathrm{sw}}(\hat{\boldsymbol{k}}_{\boldsymbol{t}}) \cdot \boldsymbol{\rho}} \, \mathrm{d}\hat{\boldsymbol{k}}_{\boldsymbol{t}} \\ \eta_0 \mathbf{J} \cdot \boldsymbol{H}_{xy_{\mathrm{sw}}}(\boldsymbol{\rho}, z_0) = \mathbf{W}^{-1}(\boldsymbol{k}_{t\mathrm{sw}}(\hat{\boldsymbol{k}}_{\boldsymbol{t}})) \cdot \boldsymbol{E}_{xy_{\mathrm{sw}}}(\boldsymbol{\rho}, z_0) \end{cases} \tag{3.9}$$

where $\mathbf{A}_{-1}(k_{t\mathrm{sw}}(\hat{\boldsymbol{k}}_{\boldsymbol{t}}))$ denotes the residue of the $\mathbf{T}_{22}$ dyadic along the direction $\hat{\boldsymbol{k}}_{\boldsymbol{t}}$, see (C.1).

The electric field at an arbitrary position in the slab is obtained from the field at $z = z_0$ by the use of the propagators, (2.4)

$$\begin{cases} \boldsymbol{E}_{xy_{\mathrm{sw}}}(\boldsymbol{\rho}, z) = \dfrac{\mathrm{i}}{2\pi} \displaystyle\int_0^{2\pi} \left(\mathbf{P}_{11}(\boldsymbol{k}_{t\mathrm{sw}}(\hat{\boldsymbol{k}}_{\boldsymbol{t}}), z, z_0) + \mathbf{P}_{12}(\boldsymbol{k}_{t\mathrm{sw}}(\hat{\boldsymbol{k}}_{\boldsymbol{t}}), z, z_0) \cdot \mathbf{W}^{-1}(\boldsymbol{k}_{t\mathrm{sw}}(\hat{\boldsymbol{k}}_{\boldsymbol{t}})) \right) \\ \qquad \cdot \mathbf{A}_{-1}(k_{t\mathrm{sw}}(\hat{\boldsymbol{k}}_{\boldsymbol{t}})) \cdot \left\{ \boldsymbol{F}^-(\boldsymbol{k}_{t\mathrm{sw}}(\hat{\boldsymbol{k}}_{\boldsymbol{t}}), z_1) - \mathbf{T}_{21}(\boldsymbol{k}_{t\mathrm{sw}}(\hat{\boldsymbol{k}}_{\boldsymbol{t}})) \cdot \boldsymbol{F}^+(\boldsymbol{k}_{t\mathrm{sw}}(\hat{\boldsymbol{k}}_{\boldsymbol{t}}), z_0) \right\} \\ \qquad \cdot \mathrm{e}^{\mathrm{i}\boldsymbol{k}_{t\mathrm{sw}}(\hat{\boldsymbol{k}}_{\boldsymbol{t}}) \cdot \boldsymbol{\rho}} \, \mathrm{d}\hat{\boldsymbol{k}}_{\boldsymbol{t}} \end{cases} \tag{3.10}$$

Notice that these surface waves cannot be excited by an incident plane wave, since the surface wave always has a transverse wave number that satisfies $|\boldsymbol{k}_{t\mathrm{sw}}| \geq k_0$, *i.e.*, the wave is evanescent outside the slab. The incident plane wave, however, must be a propagating wave satisfying $|\boldsymbol{k}_t| \leq k_0$, and, therefore, the exciting fields $\boldsymbol{F}^+(\boldsymbol{k}_t, z_0)$ and $\boldsymbol{F}^-(\boldsymbol{k}_t, z_1)$ have only support in this region. A source, *e.g.*, a dipole or a periodic metallic pattern (FSS), which has a broader plane wave spectrum can be used to excite the surface wave.

3.5 ODE for the dyadic T

It is possible to find an ODE for the dyadic $\mathbf{T}$. This is valuable in the computations of the residues of the field. To proceed, denote

$$\mathbf{T}(z) = \mathbf{S} \cdot \mathbf{P}(z, z_0) \cdot \mathbf{S}^{-1}$$

with initial value

$$\mathbf{T}(z_0) = \mathbf{I}_4$$

We note that

$$\mathbf{T}_{22} = \frac{1}{2}\left(\mathbf{P}_{11} + \mathbf{W} \cdot \mathbf{P}_{21} + (\mathbf{P}_{12} + \mathbf{W} \cdot \mathbf{P}_{22}) \cdot \mathbf{W}^{-1}\right) = \frac{1}{2}\begin{pmatrix}\mathbf{I}_2 & \mathbf{W}\end{pmatrix} \cdot \mathbf{P} \cdot \begin{pmatrix}\mathbf{I}_2 \\ \mathbf{W}^{-1}\end{pmatrix}$$

By the use of (2.5)

$$\frac{\mathrm{d}}{\mathrm{d}z}\mathbf{P}(z, z_0) = \mathrm{i}k_0 \mathbf{M}(z) \cdot \mathbf{P}(z, z_0)$$

we get

$$\frac{\mathrm{d}}{\mathrm{d}z}\mathbf{T}(z) = \mathrm{i}k_0 \mathbf{S} \cdot \mathbf{M}(z) \cdot \mathbf{P}(z, z_0) \cdot \mathbf{S}^{-1}$$

which implies

$$\frac{\mathrm{d}}{\mathrm{d}z}\mathbf{T}(z) = \mathrm{i}k_0 \mathbf{S} \cdot \mathbf{M}(z) \cdot \mathbf{S}^{-1} \cdot \mathbf{T}(z) = \mathrm{i}k_0 \mathbf{C}(z) \cdot \mathbf{T}(z)$$

Here the two-dimensional components $\mathbf{C}_{ij}$, $i, j = 1, 2$, of the four-dimensional dyadic $\mathbf{C}$ are related as

$$\begin{cases} 2\mathbf{C}_{11} = \left(\mathbf{M}_{11} - \mathbf{M}_{12} \cdot \mathbf{W}^{-1}\right) - \mathbf{W} \cdot \left(\mathbf{M}_{21} - \mathbf{M}_{22} \cdot \mathbf{W}^{-1}\right) \\ 2\mathbf{C}_{12} = \left(\mathbf{M}_{11} + \mathbf{M}_{12} \cdot \mathbf{W}^{-1}\right) - \mathbf{W} \cdot \left(\mathbf{M}_{21} + \mathbf{M}_{22} \cdot \mathbf{W}^{-1}\right) \\ 2\mathbf{C}_{21} = \left(\mathbf{M}_{11} - \mathbf{M}_{12} \cdot \mathbf{W}^{-1}\right) + \mathbf{W} \cdot \left(\mathbf{M}_{21} - \mathbf{M}_{22} \cdot \mathbf{W}^{-1}\right) \\ 2\mathbf{C}_{22} = \left(\mathbf{M}_{11} + \mathbf{M}_{12} \cdot \mathbf{W}^{-1}\right) + \mathbf{W} \cdot \left(\mathbf{M}_{21} + \mathbf{M}_{22} \cdot \mathbf{W}^{-1}\right) \end{cases}$$

The surface waves are determined by the transverse wave numbers $\boldsymbol{k}_{t\mathrm{sw}}(\hat{\boldsymbol{k}_t})$ that satisfy

$$\begin{cases} \dfrac{\mathrm{d}}{\mathrm{d}z}\mathbf{T}(\boldsymbol{k}_{t\mathrm{sw}}, z) = \mathrm{i}k_0 \mathbf{C}(\boldsymbol{k}_{t\mathrm{sw}}, z) \cdot \mathbf{T}(\boldsymbol{k}_{t\mathrm{sw}}, z) \\ \mathbf{T}(\boldsymbol{k}_{t\mathrm{sw}}, z_0) = \mathbf{I}_4 \\ \mathbf{T}_{22}(\boldsymbol{k}_{t\mathrm{sw}}, z_1) \text{ singular} \end{cases}$$

3.6 Onset of the surface field

The onset of the surface field is characterized by a transversal wave number $|\boldsymbol{k}_t| = k_0$. Therefore, the condition for the onset of a surface mode is the existence of zero eigenvalue of $\mathbf{T}_{22}(k_t = k_0, d, 0)$. Due to the behavior of the splitting dyadic $\mathbf{W}$ for arguments close to $k_t = k_0$, see (2.8) and (2.9), we get the following necessary condition of the onset (arguments $|\boldsymbol{k}_t| = k_0$)

$$\hat{\boldsymbol{e}}_\perp \left(\hat{\boldsymbol{e}}_\perp \cdot \mathbf{P}_{21}\right) + \left(\mathbf{P}_{12} \cdot \hat{\boldsymbol{e}}_\parallel\right) \hat{\boldsymbol{e}}_\parallel + \hat{\boldsymbol{e}}_\perp \left(\hat{\boldsymbol{e}}_\perp \cdot \mathbf{P}_{22} \cdot \hat{\boldsymbol{e}}_\parallel\right) \hat{\boldsymbol{e}}_\parallel = \mathbf{0} \tag{3.11}$$

4 Examples

Before proceeding to a geometry with metal screens in Section 5, we illustrate the theory in Section 3 with a few examples.

4.1 Inhomogeneous, isotropic material

The isotropic case is the most important case in radome applications, and in this section we specialize to this material class. The material parameters in this class of material are characterized by the relative permittivity $\epsilon(z)$ and the relative permeability $\mu(z)$. The longitudinal components of the fields in an isotropic material are related to the transverse components of the fields as, see (2.3)

$$\begin{cases} E_z(z) = \dfrac{\boldsymbol{k}_t \cdot \eta_0 \mathbf{J} \cdot \boldsymbol{H}_{xy}(z)}{k_0 \epsilon(z)} \\ \eta_0 H_z(z) = \dfrac{\mathbf{J} \cdot \boldsymbol{k}_t \cdot \boldsymbol{E}_{xy}(z)}{k_0 \mu(z)} \end{cases}$$

In a isotropic material the propagators is diagonal in the basis $\{\hat{\boldsymbol{e}}_\parallel, \hat{\boldsymbol{e}}_\perp\}$, *i.e.*,

$$\begin{cases} \mathbf{P}_{ij}(z_1, z_0) = P_{ij}^{\mathrm{TM}}(z_1, z_0)\hat{\boldsymbol{e}}_\parallel\hat{\boldsymbol{e}}_\parallel + P_{ij}^{\mathrm{TE}}(z_1, z_0)\hat{\boldsymbol{e}}_\perp\hat{\boldsymbol{e}}_\perp \\ \mathbf{T}_{ij}(z_1, z_0) = T_{ij}^{\mathrm{TM}}(z_1, z_0)\hat{\boldsymbol{e}}_\parallel\hat{\boldsymbol{e}}_\parallel + T_{ij}^{\mathrm{TE}}(z_1, z_0)\hat{\boldsymbol{e}}_\perp\hat{\boldsymbol{e}}_\perp \end{cases} \qquad i, j = 1, 2$$

where the T_{ij}-components, $i, j = 1, 2$, are expressed in the propagator components P_{ij}-components, $i, j = 1, 2$, as (see (2.8) and (2.9))

$$\begin{cases} 2T_{21}^{\mathrm{TM}} = P_{11}^{\mathrm{TM}} + \dfrac{k_z}{k_0}P_{21}^{\mathrm{TM}} - \dfrac{k_0}{k_z}P_{12}^{\mathrm{TM}} - P_{22}^{\mathrm{TM}} \\ 2T_{21}^{\mathrm{TE}} = P_{11}^{\mathrm{TE}} + \dfrac{k_0}{k_z}P_{21}^{\mathrm{TE}} - \dfrac{k_z}{k_0}P_{12}^{\mathrm{TE}} - P_{22}^{\mathrm{TE}} \end{cases}$$

and

$$\begin{cases} 2T_{22}^{\mathrm{TM}} = P_{11}^{\mathrm{TM}} + \dfrac{k_z}{k_0}P_{21}^{\mathrm{TM}} + \dfrac{k_0}{k_z}P_{12}^{\mathrm{TM}} + P_{22}^{\mathrm{TM}} \\ 2T_{22}^{\mathrm{TE}} = P_{11}^{\mathrm{TE}} + \dfrac{k_0}{k_z}P_{21}^{\mathrm{TE}} + \dfrac{k_z}{k_0}P_{12}^{\mathrm{TE}} + P_{22}^{\mathrm{TE}} \end{cases} \tag{4.1}$$

The ODE for the propagators in the TM-case are [6]

$$\begin{cases} \dfrac{\mathrm{d}}{\mathrm{d}z}P_{11}^{\mathrm{TM}} = \mathrm{i}k_0\left(\dfrac{k_t^2}{k_0^2\epsilon(z)} - \mu(z)\right)P_{21}^{\mathrm{TM}} \\ \dfrac{\mathrm{d}}{\mathrm{d}z}P_{21}^{\mathrm{TM}} = -\mathrm{i}k_0\epsilon(z)P_{11}^{\mathrm{TM}} \end{cases} \qquad \begin{cases} P_{11}^{\mathrm{TM}}(z_1, z_1) = 1 \\ P_{21}^{\mathrm{TM}}(z_1, z_1) = 0 \end{cases}$$

and

$$\begin{cases} \dfrac{\mathrm{d}}{\mathrm{d}z}P_{12}^{\mathrm{TM}} = \mathrm{i}k_0\left(\dfrac{k_t^2}{k_0^2\epsilon(z)} - \mu(z)\right)P_{22}^{\mathrm{TM}} \\ \dfrac{\mathrm{d}}{\mathrm{d}z}P_{22}^{\mathrm{TM}} = -\mathrm{i}k_0\epsilon(z)P_{12}^{\mathrm{TM}} \end{cases} \qquad \begin{cases} P_{12}^{\mathrm{TM}}(z_1, z_1) = 0 \\ P_{22}^{\mathrm{TM}}(z_1, z_1) = 1 \end{cases}$$

Note that the equations are identical, but the initial conditions differ.

For the other polarization, $\perp$-polarization, we obtain the TE-case, which also splits in two non-coupling sets of first order ordinary differential equations.

$$\begin{cases} \dfrac{\mathrm{d}}{\mathrm{d}z}P_{11}^{\mathrm{TE}} = -\mathrm{i}k_0\mu(z)P_{21}^{\mathrm{TE}} \\ \dfrac{\mathrm{d}}{\mathrm{d}z}P_{21}^{\mathrm{TE}} = \mathrm{i}k_0\left(\dfrac{k_t^2}{k_0^2\mu(z)} - \epsilon(z)\right)P_{11}^{\mathrm{TE}} \end{cases} \qquad \begin{cases} P_{11}^{\mathrm{TE}}(z_1, z_1) = 1 \\ P_{21}^{\mathrm{TE}}(z_1, z_1) = 0 \end{cases}$$

and

$$\begin{cases} \dfrac{\mathrm{d}}{\mathrm{d}z}P_{12}^{\mathrm{TE}} = -\mathrm{i}k_0\mu(z)P_{22}^{\mathrm{TE}} \\ \dfrac{\mathrm{d}}{\mathrm{d}z}P_{22}^{\mathrm{TE}} = \mathrm{i}k_0\left(\dfrac{k_t^2}{k_0^2\mu(z)} - \epsilon(z)\right)P_{12}^{\mathrm{TE}} \end{cases} \qquad \begin{cases} P_{12}^{\mathrm{TE}}(z_1, z_1) = 0 \\ P_{22}^{\mathrm{TE}}(z_1, z_1) = 1 \end{cases}$$

Again, the equations are identical, but the initial conditions differ.

The general behavior of these solutions are found by diagonalizing the matrices. Also the high frequency behavior is possible to find, see *e.g.*, [11].

4.1.1 Onset of surface waves

For an isotropic material, the singular values, $\boldsymbol{k}_{t\mathrm{sw}}$, are independent of the direction $\hat{\boldsymbol{k}_t}$, and the $\boldsymbol{k}_t$-value for onset satisfies $k_t = k_0$, or stated differently $k_z = 0$ at this frequency. Therefore, the condition for the onset of a surface mode, $T_{22}^{\mathrm{TM,\ TE}}(k_t = k_0, d, 0) = 0$, is different for the TM- and the TE-cases. At onset, due to (4.1), a necessary condition is

$$\begin{cases} P_{12}^{\mathrm{TM}}(k_t = k_0, z_1, z_0) = 0 \\ P_{21}^{\mathrm{TE}}(k_t = k_0, z_1, z_0) = 0 \end{cases}$$

which also is consistent with the general expression for the onset of surface waves in (3.11). These conditions are the general conditions for the onset of a surface wave if the isotropic material is inhomogeneous w.r.t. the depth parameter z.

4.2 Homogeneous, isotropic material

If the isotropic material is homogeneous, then all systems are analytically solvable. This case is found in the literature, *e.g.*, [1], but employing a different method.

For a homogeneous, isotropic material, the propagators are ($d = z_1 - z_0$) [9, 10]

$$\begin{cases} \mathbf{P}_{11}(z_1, z_0) = \mathbf{I}_2 \cos(k_0 \kappa d) \\ \mathbf{P}_{12}(z_1, z_0) = -\dfrac{\mathrm{i}}{\kappa} \sin(k_0 \kappa d) \left\{ \dfrac{\kappa^2}{\epsilon} \hat{\boldsymbol{e}}_\parallel \hat{\boldsymbol{e}}_\parallel + \mu \hat{\boldsymbol{e}}_\perp \hat{\boldsymbol{e}}_\perp \right\} \\ \mathbf{P}_{21}(z_1, z_0) = -\dfrac{\mathrm{i}}{\kappa} \sin(k_0 \kappa d) \left\{ \epsilon \hat{\boldsymbol{e}}_\parallel \hat{\boldsymbol{e}}_\parallel + \dfrac{\kappa^2}{\mu} \hat{\boldsymbol{e}}_\perp \hat{\boldsymbol{e}}_\perp \right\} \\ \mathbf{P}_{22}(z_1, z_0) = \mathbf{I}_2 \cos(k_0 \kappa d) \end{cases}$$

where $\kappa^2 = \epsilon\mu - k_t^2/k_0^2$. We also have, see (2.8) and (2.9)

$$\mathbf{W}(\boldsymbol{k}_t) = \frac{k_z}{k_0} \hat{\boldsymbol{e}}_\parallel \hat{\boldsymbol{e}}_\parallel + \frac{k_0}{k_z} \hat{\boldsymbol{e}}_\perp \hat{\boldsymbol{e}}_\perp, \qquad \mathbf{W}^{-1}(\boldsymbol{k}_t) = \frac{k_0}{k_z} \hat{\boldsymbol{e}}_\parallel \hat{\boldsymbol{e}}_\parallel + \frac{k_z}{k_0} \hat{\boldsymbol{e}}_\perp \hat{\boldsymbol{e}}_\perp$$

which implies

$$\begin{cases} 2T_{22}^{\mathrm{TM}} = 2\cos(k_0 \kappa d) - \dfrac{k_z}{k_0} \dfrac{\mathrm{i}\epsilon}{\kappa} \sin(k_0 \kappa d) - \dfrac{k_0}{k_z} \dfrac{\mathrm{i}\kappa}{\epsilon} \sin(k_0 \kappa d) \\ 2T_{22}^{\mathrm{TE}} = 2\cos(k_0 \kappa d) - \dfrac{k_0}{k_z} \dfrac{\mathrm{i}\kappa}{\mu} \sin(k_0 \kappa d) - \dfrac{k_z}{k_0} \dfrac{\mathrm{i}\mu}{\kappa} \sin(k_0 \kappa d) \end{cases}$$

Denote $x = k_{t\mathrm{sw}}/k_0 > 0$. Then $\kappa^2 = \epsilon\mu - x^2$ and $k_z/k_0 = \mathrm{i}\sqrt{x^2 - 1}$ and the conditions for a surface wave become

$$\begin{cases} \dfrac{\epsilon}{\kappa} \sqrt{x^2 - 1} \tan(k_0 \kappa d) - \dfrac{\kappa}{\epsilon \sqrt{x^2 - 1}} \tan(k_0 \kappa d) + 2 = 0, & \text{TM-case} \\ \dfrac{\mu}{\kappa} \sqrt{x^2 - 1} \tan(k_0 \kappa d) - \dfrac{\kappa}{\mu \sqrt{x^2 - 1}} \tan(k_0 \kappa d) + 2 = 0, & \text{TE-case} \end{cases}$$

The onset is explicitly given by

$$k_0 d = \frac{2n\pi}{2\sqrt{\epsilon\mu - 1}}, \qquad n = 1, 2, 3, 4, \ldots$$

To compare with the solution obtained with other methods, we rewrite the equations in terms of half of the arguments in the trigonometric functions. We get

$$\begin{cases} \left(\tan(k_0 \kappa d/2) - \dfrac{\epsilon}{\kappa} \sqrt{x^2 - 1} \right) \left(\tan(k_0 \kappa d/2) + \dfrac{\kappa}{\epsilon \sqrt{x^2 - 1}} \right) = 0, & \text{TM-case} \\ \left(\tan(k_0 \kappa d/2) - \dfrac{\mu}{\kappa} \sqrt{x^2 - 1} \right) \left(\tan(k_0 \kappa d/2) + \dfrac{\kappa}{\mu \sqrt{x^2 - 1}} \right) = 0, & \text{TE-case} \end{cases}$$

with solutions (only solutions $x > 0$ are sought)

$$\begin{cases} \tan(k_0\kappa d/2) = \dfrac{\epsilon\sqrt{x^2-1}}{\kappa} = \dfrac{\epsilon\sqrt{\epsilon\mu-1-\kappa^2}}{\kappa}, & \text{even TM-case} \\ \cot(k_0\kappa d/2) = -\dfrac{\epsilon\sqrt{x^2-1}}{\kappa} = -\dfrac{\epsilon\sqrt{\epsilon\mu-1-\kappa^2}}{\kappa}, & \text{odd TM-case} \\ \tan(k_0\kappa d/2) = \dfrac{\mu\sqrt{x^2-1}}{\kappa} = \dfrac{\mu\sqrt{\epsilon\mu-1-\kappa^2}}{\kappa}, & \text{even TE-case} \\ \cot(k_0\kappa d/2) = -\dfrac{\mu\sqrt{x^2-1}}{\kappa} = -\dfrac{\mu\sqrt{\epsilon\mu-1-\kappa^2}}{\kappa}, & \text{odd TE-case} \end{cases} \tag{4.2}$$

which agree with the well known results obtained by other methods [1]. The quantitative behavior of the solutions of these equations can be seen graphically. To this end, introduce the variables

$$\begin{cases} u = k_0\kappa d/2 = k_0\sqrt{\epsilon\mu - x^2}\,d/2 \\ v = k_0\sqrt{x^2-1}\,d/2 \end{cases}$$

and (4.2) becomes

$$\begin{cases} v = \dfrac{u\tan u}{\epsilon}, & \text{even TM-case} \\ v = -\dfrac{u\cot u}{\epsilon}, & \text{odd TM-case} \\ v = \dfrac{u\tan u}{\mu}, & \text{even TE-case} \\ v = -\dfrac{u\cot u}{\mu}, & \text{odd TE-case} \end{cases} \tag{4.3}$$

We plot these functions in a u-v-diagram and observe that the variables u and v are connected by

$$u^2 + v^2 = k_0^2(\epsilon\mu - 1)d^2/4 \tag{4.4}$$

which is a circle in the u-v-plane with radius $k_0\sqrt{\epsilon\mu-1}\,d/2$. Two illustrations, see Figures 2 and 3, illustrate the existence of a surface wave for the discrete x-values ($x > 0$) at the intersections between the curves in (4.3) and the circles in (4.4) determined by the frequency and the thickness of the slab.

The dispersion curves relate the frequency of the surface wave and the transverse wave number of the surface wave. An example of such a calculation for a homogeneous, isotropic material is shown in Figures 4–6.

4.2.1 The electric field and its symmetries

In this section we investigate the relation between the surface waves obtained above and the surface waves in the presence of a ground plane. These latter waves are also investigated in Ref. 6.

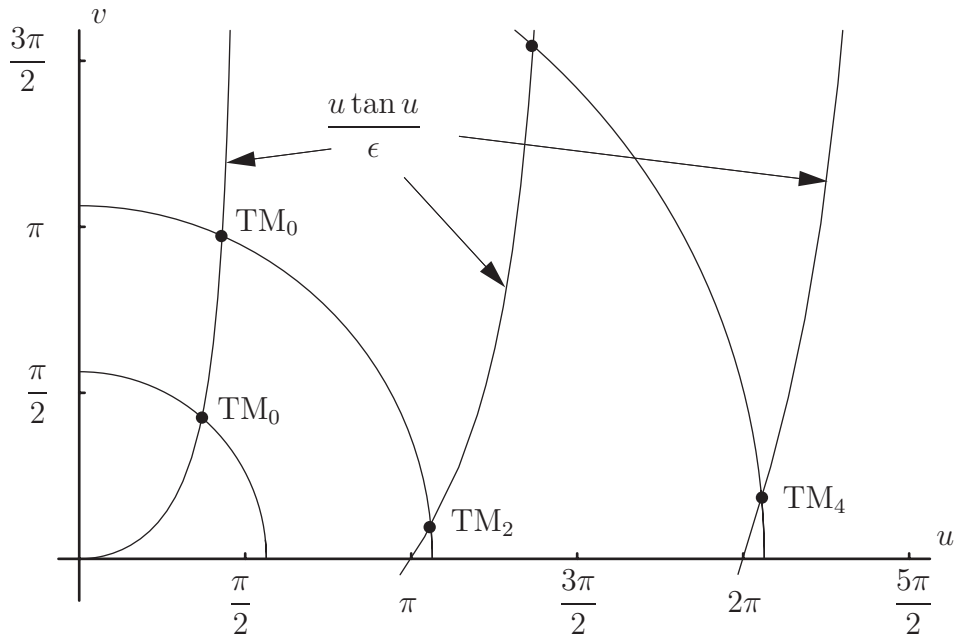

Figure 2: Geometrical characterization of even TM-modes for $\epsilon = 2$ and $\mu = 1$. The surface modes are determined by the x-values at the intersections of the curve $v = u \tan u/\epsilon$ and the circle in (4.4). The radius of the circle is $k_0\sqrt{\epsilon\mu - 1}d/2$.

To determine the electric field of the surface field, see (3.9), we need to compute $\mathbf{P}_{11}(\boldsymbol{k}_t, z, z_0) + \mathbf{P}_{12}(\boldsymbol{k}_t, z, z_0) \cdot \mathbf{W}^{-1}(\boldsymbol{k}_t)$. This is readily done by observing that

$$\begin{aligned}
&\mathbf{P}_{11}(\boldsymbol{k}_t, z, z_0) + \mathbf{P}_{12}(\boldsymbol{k}_t, z, z_0) \cdot \mathbf{W}^{-1}(\boldsymbol{k}_t) \\
&\qquad = \mathbf{I}_2 \cos\left(k_0\kappa(z - z_0)\right) - \frac{\mathrm{i}}{\kappa} \sin\left(k_0\kappa(z - z_0)\right) \left\{ \frac{\kappa^2}{\epsilon} \frac{k_0}{k_z} \hat{\boldsymbol{e}}_\parallel \hat{\boldsymbol{e}}_\parallel + \mu \frac{k_z}{k_0} \hat{\boldsymbol{e}}_\perp \hat{\boldsymbol{e}}_\perp \right\}
\end{aligned}$$

If we evaluate at the midpoint of the slab $z_m = (z_0 + z_1)/2$, we obtain

$$\begin{aligned}
&\mathbf{P}_{11}(\boldsymbol{k}_t, z_m, z_0) + \mathbf{P}_{12}(\boldsymbol{k}_t, z_m, z_0) \cdot \mathbf{W}^{-1}(\boldsymbol{k}_t) \\
&= \mathbf{I}_2 \cos\left(k_0\kappa d/2\right) - \frac{\mathrm{i}}{\kappa} \sin\left(k_0\kappa d/2\right) \left\{ \frac{\kappa^2}{\epsilon} \frac{k_0}{k_z} \hat{\boldsymbol{e}}_\parallel \hat{\boldsymbol{e}}_\parallel + \mu \frac{k_z}{k_0} \hat{\boldsymbol{e}}_\perp \hat{\boldsymbol{e}}_\perp \right\} \\
&= \cos\left(k_0\kappa d/2\right) \left(\mathbf{I}_2 - \frac{\mathrm{i}}{\kappa} \tan\left(k_0\kappa d/2\right) \left\{ \frac{\kappa^2}{\epsilon} \frac{1}{\mathrm{i}\sqrt{x^2 - 1}} \hat{\boldsymbol{e}}_\parallel \hat{\boldsymbol{e}}_\parallel + \mu \mathrm{i}\sqrt{x^2 - 1} \hat{\boldsymbol{e}}_\perp \hat{\boldsymbol{e}}_\perp \right\} \right)
\end{aligned}$$

The characteristic equations in (4.2) imply for the even TM-case

$$\left(\mathbf{P}_{11}(\boldsymbol{k}_t, z_m, z_0) + \mathbf{P}_{12}(\boldsymbol{k}_t, z_m, z_0) \cdot \mathbf{W}^{-1}(\boldsymbol{k}_t)\right) \cdot \hat{\boldsymbol{e}}_\parallel = \mathbf{0}$$

and for the odd TE-case

$$\left(\mathbf{P}_{11}(\boldsymbol{k}_t, z_m, z_0) + \mathbf{P}_{12}(\boldsymbol{k}_t, z_m, z_0) \cdot \mathbf{W}^{-1}(\boldsymbol{k}_t)\right) \cdot \hat{\boldsymbol{e}}_\perp = \mathbf{0}$$

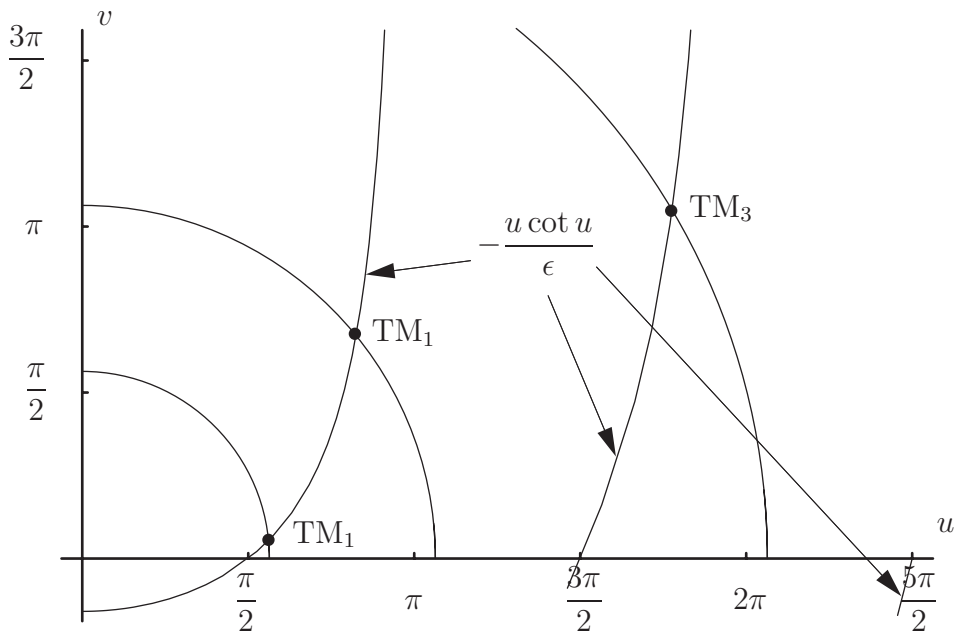

Figure 3: Geometrical characterization of odd TM-modes for $\epsilon = 2$ and $\mu = 1$. The surface modes are determined by the x-values at the intersections of the curve $v = -u\cot u/\epsilon$ and the circle in (4.4). The radius of the circle is $k_0\sqrt{\epsilon\mu - 1}d/2$.

From (3.9) and (3.10), we get

$$\boldsymbol{E}_{xy_{\rm sw}}(\boldsymbol{r})\big|_{z=z_m} = \big(\mathbf{P}_{11}(\boldsymbol{k}_{t\rm sw}, z_m, z_0) + \mathbf{P}_{12}(\boldsymbol{k}_{t\rm sw}, z_m, z_0)\cdot\mathbf{W}^{-1}(\boldsymbol{k}_{t\rm sw})\big)\cdot\boldsymbol{E}_{xy_{\rm sw}}(\boldsymbol{\rho}, z_0)$$

which implies

$$\begin{cases} \boldsymbol{E}_{xy_{\rm sw}}(\boldsymbol{r})\big|_{z=z_m}\cdot\hat{\boldsymbol{e}}_{\parallel} = \mathbf{0}, & \text{even TM-case} \\ \boldsymbol{E}_{xy_{\rm sw}}(\boldsymbol{r})\big|_{z=z_m}\cdot\hat{\boldsymbol{e}}_{\perp} = \mathbf{0}, & \text{odd TE-case} \end{cases}$$

since in the TM-case the electric field is polarized along the $\hat{\boldsymbol{e}}_{\parallel}$-direction and in the TE-case perpendicular to this direction. Therefore, the even TM-case and the odd TE-case give the surface waves for a grounded slab of half the thickness. The onset frequencies are determined by

$$k_0 d/2 = \frac{2n\pi}{2\sqrt{\epsilon\mu - 1}}, \qquad n = 0, 1, 2, 3, \ldots, \quad \text{even TM-case}$$

and

$$k_0 d/2 = \frac{(2n+1)\pi}{2\sqrt{\epsilon\mu - 1}}, \qquad n = 0, 1, 2, 3, \ldots, \quad \text{odd TE-case}$$

respectively.

4.3 Uniaxial material

The permittivity dyadic of the uniaxial medium can be written as

$$\epsilon = \epsilon_1\,(\mathbf{I}_3 - \hat{\boldsymbol{u}}\hat{\boldsymbol{u}}) + \epsilon_2\hat{\boldsymbol{u}}\hat{\boldsymbol{u}}$$

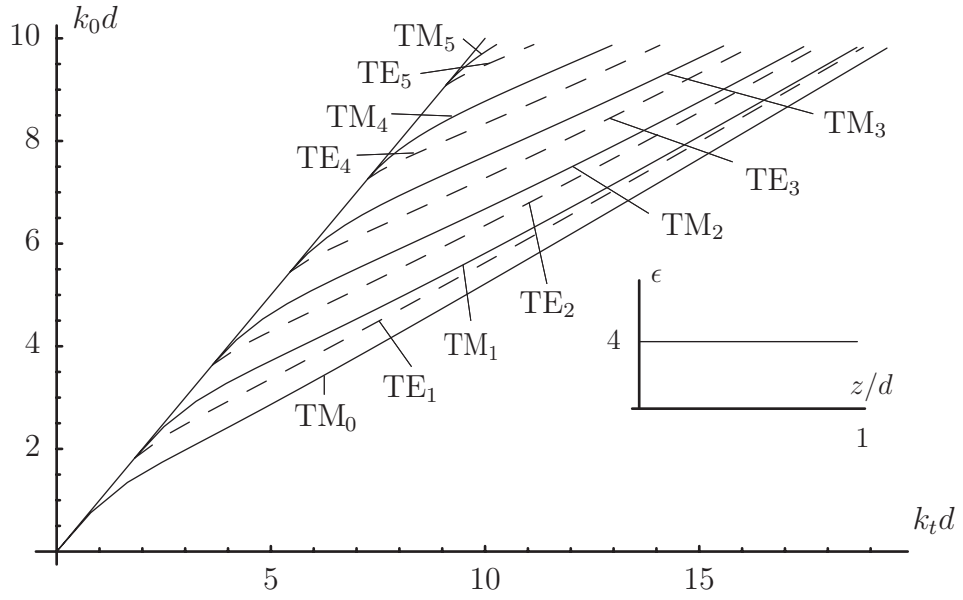

Figure 4: The normalized frequency $k_0 d = \omega d/c_0$ as a function of the normalized wave number $k_t d$ of the surface mode. The figure shows the dispersion curves for an isotropic profile $\epsilon = 4$ and $\mu = 1$. The $k_0 d$-values for the onset of the different modes for the profile are: $\mathrm{TE}_1 = \mathrm{TM}_1 = 1.81$, $\mathrm{TE}_2 = \mathrm{TM}_2 = 3.63$, $\mathrm{TE}_3 = \mathrm{TM}_3 = 5.44$, $\mathrm{TE}_4 = \mathrm{TM}_4 = 7.26$, and $\mathrm{TE}_5 = \mathrm{TM}_5 = 9.07$. The solid lines show the TM-modes and the dashed lines the TE-modes.

where the unit vector $\hat{\boldsymbol{u}}$ defines an optical axis in the material. The single-slab propagator for a homogeneous, non-magnetic, uniaxial slab with the optical axis in the $\hat{\boldsymbol{u}} = \hat{\boldsymbol{z}}$-direction is given by [9]

$$\begin{cases} \mathbf{P}_{11}(z_1, z_0) = \hat{\boldsymbol{e}}_{\parallel}\hat{\boldsymbol{e}}_{\parallel}\cos(k_0 d\lambda_-) + \hat{\boldsymbol{e}}_{\perp}\hat{\boldsymbol{e}}_{\perp}\cos(k_0 d\lambda_+) \\ \mathbf{P}_{12}(z_1, z_0) = -i\hat{\boldsymbol{e}}_{\parallel}\hat{\boldsymbol{e}}_{\parallel}\dfrac{\lambda_-}{\epsilon_1}\sin(k_0 d\lambda_-) - i\hat{\boldsymbol{e}}_{\perp}\hat{\boldsymbol{e}}_{\perp}\dfrac{1}{\lambda_+}\sin(k_0 d\lambda_+) \\ \mathbf{P}_{21}(z_1, z_0) = -i\hat{\boldsymbol{e}}_{\parallel}\hat{\boldsymbol{e}}_{\parallel}\dfrac{\epsilon_1}{\lambda_-}\sin(k_0 d\lambda_-) - i\hat{\boldsymbol{e}}_{\perp}\hat{\boldsymbol{e}}_{\perp}\lambda_+\sin(k_0 d\lambda_+) \\ \mathbf{P}_{22}(z_1, z_0) = \hat{\boldsymbol{e}}_{\parallel}\hat{\boldsymbol{e}}_{\parallel}\cos(k_0 d\lambda_-) + \hat{\boldsymbol{e}}_{\perp}\hat{\boldsymbol{e}}_{\perp}\cos(k_0 d\lambda_+) \end{cases}$$

where the four eigenvalues of $\mathbf{M}$, $\pm\lambda_\pm$ are all distinct; specifically

$$\lambda_+^2 = \epsilon_1 - \frac{k_t^2}{k_0^2}, \qquad \lambda_-^2 = \epsilon_1 - \frac{k_t^2}{k_0^2}\frac{\epsilon_1}{\epsilon_2}$$

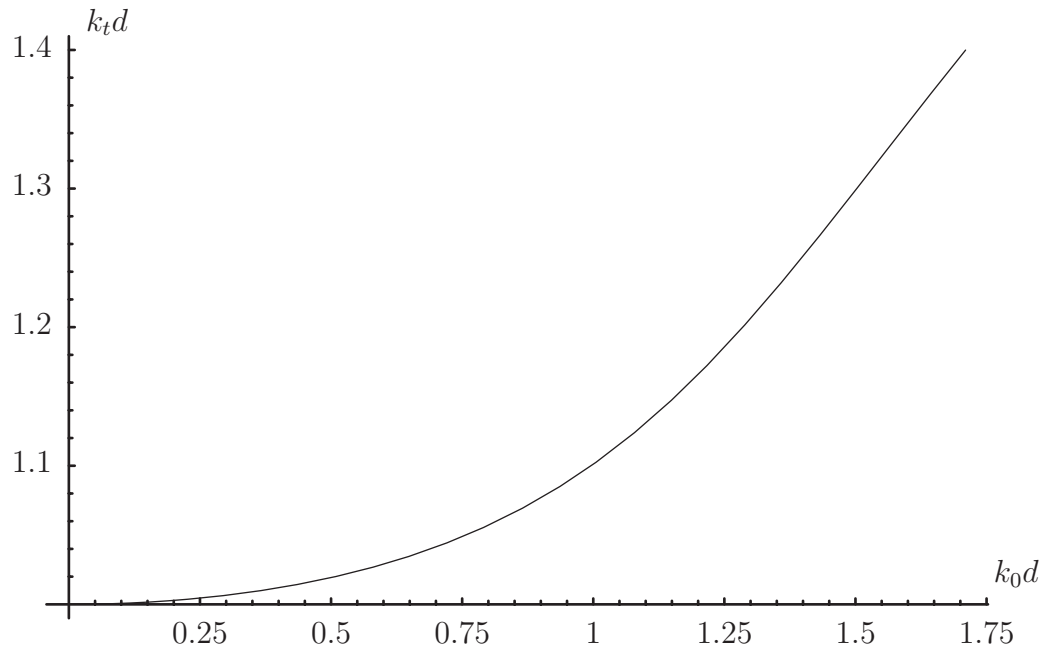

Figure 5: The normalized wave number $k_t d$ of the surface wave as a function of the normalized frequency $k_0 d$ of the TM_0-mode for an isotropic profile $\epsilon = 4$ and $\mu = 1$.

We proceed by computing

$$\begin{aligned}
2\mathbf{T}_{22} =& \mathbf{P}_{11} + \mathbf{W}\cdot\mathbf{P}_{21} + (\mathbf{P}_{12} + \mathbf{W}\cdot\mathbf{P}_{22})\cdot\mathbf{W}^{-1} \\
=& \hat{\boldsymbol{e}}_{\parallel}\hat{\boldsymbol{e}}_{\parallel}\cos(k_0 d\lambda_-) + \hat{\boldsymbol{e}}_{\perp}\hat{\boldsymbol{e}}_{\perp}\cos(k_0 d\lambda_+) \\
& - i\frac{k_z}{k_0}\hat{\boldsymbol{e}}_{\parallel}\hat{\boldsymbol{e}}_{\parallel}\frac{\epsilon_1}{\lambda_-}\sin(k_0 d\lambda_-) - i\frac{k_0}{k_z}\hat{\boldsymbol{e}}_{\perp}\hat{\boldsymbol{e}}_{\perp}\lambda_+\sin(k_0 d\lambda_+) \\
& - i\frac{k_0}{k_z}\hat{\boldsymbol{e}}_{\parallel}\hat{\boldsymbol{e}}_{\parallel}\frac{\lambda_-}{\epsilon_1}\sin(k_0 d\lambda_-) - i\frac{k_z}{k_0}\hat{\boldsymbol{e}}_{\perp}\hat{\boldsymbol{e}}_{\perp}\frac{1}{\lambda_+}\sin(k_0 d\lambda_+)
\end{aligned}$$

which leads to an analysis that is similar to the one developed in Section 4.2.

5 Slab with one screen

We proceed our analysis by adding one metal screen to the slab at $z = z_1$, where the end points of the slab are z_0 and z_2, see Figure 7. The location of the screen can be arbitrary within the slab, $z_0 \le z_1 \le z_2$. At this stage the metal screen has finite extent. In Section 6 the extension to the periodic metallic screen (FSS) is made.

From equations (2.4) and (2.7) we get

$$\begin{pmatrix} \boldsymbol{E}_{xy}(z_1) \\ \eta_0\mathbf{J}\cdot\boldsymbol{H}_{xy}(z_1^-) \end{pmatrix} = \mathbf{P}(z_1, z_0)\cdot\mathbf{S}^{-1}\cdot\begin{pmatrix} \boldsymbol{F}^+(z_0) \\ \boldsymbol{F}^-(z_0) \end{pmatrix} \tag{5.1}$$

where the left hand side of the metallic screen is denoted z_1^-. Notice that the transverse electric field, $\boldsymbol{E}_{xy}(z_1)$, is continuous over the metallic screen, since it is

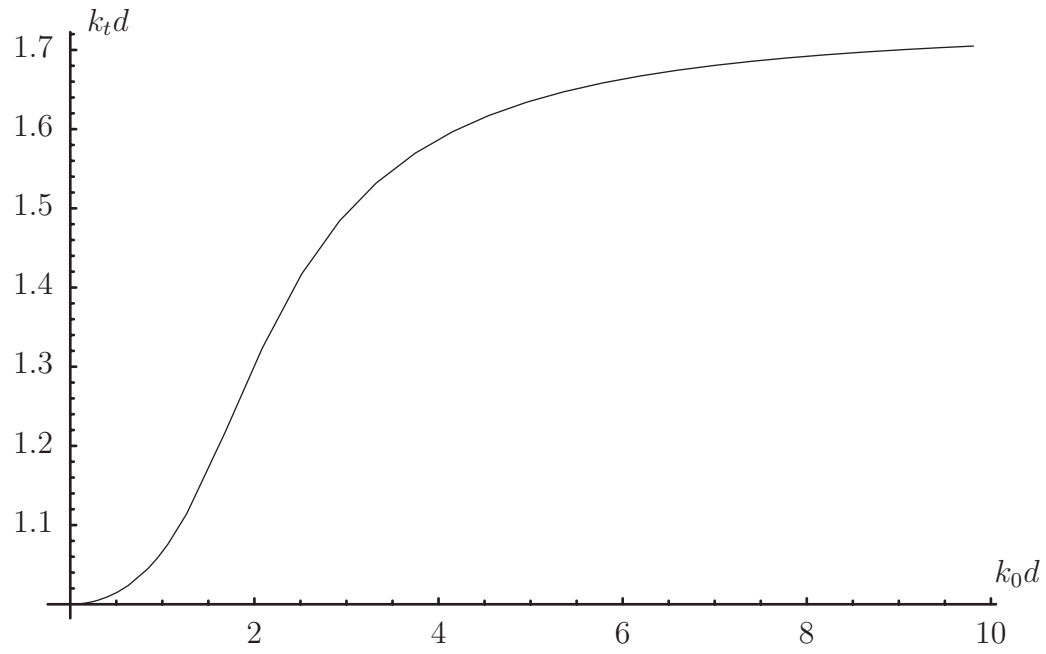

Figure 6: The normalized wave number $k_t d$ of the surface wave as a function of the normalized frequency $k_0 d$ of the TM_0-mode for an isotropic profile $\epsilon = 3$ and $\mu = 1$.

continuous outside the metallic screen and zero on the metal. Therefore, we do not have to distinguish which side of the screen the transverse electric field is evaluated.

Moreover, from equations (2.10) and (2.4)

$$\begin{aligned}\begin{pmatrix}\boldsymbol{F}^+(z_2)\\ \boldsymbol{F}^-(z_2)\end{pmatrix} =&\mathbf{S}\cdot\mathbf{P}(z_2,z_1)\cdot\begin{pmatrix}\boldsymbol{E}_{xy}(z_1)\\ \eta_0\mathbf{J}\cdot\boldsymbol{H}_{xy}(z_1^+)\end{pmatrix}\\ =&\mathbf{S}\cdot\mathbf{P}(z_2,z_1)\cdot\begin{pmatrix}\boldsymbol{E}_{xy}(z_1)\\ \eta_0\boldsymbol{J}_S(z_1)+\eta_0\mathbf{J}\cdot\boldsymbol{H}_{xy}(z_1^-)\end{pmatrix}\end{aligned}$$

where the right hand side of the metallic screen is denoted z_1^+. The surface current density $\boldsymbol{J}_S(z_1)$ is defined in the usual way as the discontinuity in the transverse magnetic field, *i.e.*,

$$\boldsymbol{J}_S(z_1) = \mathbf{J}\cdot\boldsymbol{H}_{xy}(z_1^+) - \mathbf{J}\cdot\boldsymbol{H}_{xy}(z_1^-)$$

We rewrite by the use of (5.1)

$$\begin{aligned}\begin{pmatrix}\boldsymbol{F}^+(z_2)\\ \boldsymbol{F}^-(z_2)\end{pmatrix} =&\mathbf{S}\cdot\mathbf{P}(z_2,z_1)\cdot\mathbf{P}(z_1,z_0)\cdot\mathbf{S}^{-1}\cdot\begin{pmatrix}\boldsymbol{F}^+(z_0)\\ \boldsymbol{F}^-(z_0)\end{pmatrix}\\ &+\mathbf{S}\cdot\mathbf{P}(z_2,z_1)\cdot\begin{pmatrix}\mathbf{0}\\ \eta_0\boldsymbol{J}_S(z_1)\end{pmatrix}\\ =&\mathbf{T}(z_2,z_0)\cdot\begin{pmatrix}\boldsymbol{F}^+(z_0)\\ \boldsymbol{F}^-(z_0)\end{pmatrix}+\mathbf{G}(z_2,z_1)\cdot\begin{pmatrix}\mathbf{0}\\ \eta_0\boldsymbol{J}_S(z_1)\end{pmatrix}\end{aligned}$$

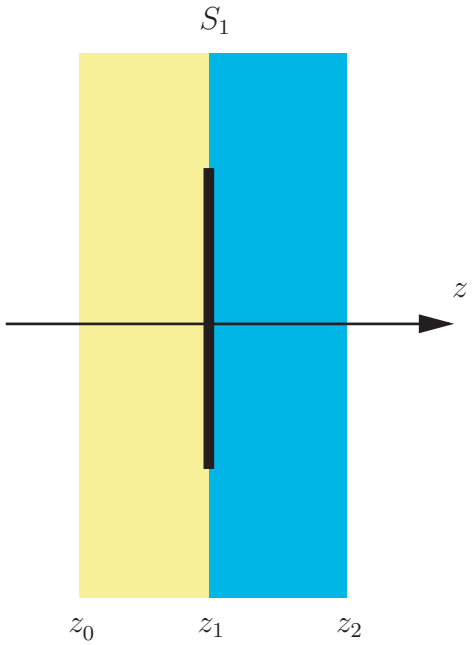

Figure 7: The geometry of the slab with one screen.

where $\mathbf{T}$ and $\mathbf{G}$ is defined in (3.3) and (3.2), respectively (the case with no screen present). In two-dimensional dyadics, we rewrite this relation as

$$\begin{cases} \boldsymbol{F}^+(z_2) = \mathbf{T}_{11}(z_2,z_0)\cdot\boldsymbol{F}^+(z_0) + \mathbf{T}_{12}(z_2,z_0)\cdot\boldsymbol{F}^-(z_0) + \mathbf{G}_{12}(z_2,z_1)\cdot\eta_0\boldsymbol{J}_S(z_1) \\ \boldsymbol{F}^-(z_0) = \mathbf{T}_{22}^{-1}(z_2,z_0)\cdot\boldsymbol{F}^-(z_2) - \mathbf{T}_{22}^{-1}(z_2,z_0)\cdot\mathbf{T}_{21}(z_2,z_0)\cdot\boldsymbol{F}^+(z_0) \\ \qquad\qquad - \mathbf{T}_{22}^{-1}(z_2,z_0)\cdot\mathbf{G}_{22}(z_2,z_1)\cdot\eta_0\boldsymbol{J}_S(z_1) \end{cases} \tag{5.2}$$

The goal is to express the fields at z_0 in terms of the excitations $\boldsymbol{F}^+(z_0)$, $\boldsymbol{F}^-(z_2)$, and $\boldsymbol{J}_S(z_1)$, *i.e.*,

$$\begin{pmatrix} \boldsymbol{E}_{xy}(z_0) \\ \eta_0\mathbf{J}\cdot\boldsymbol{H}_{xy}(z_0) \end{pmatrix} = \begin{pmatrix} \mathbf{A} & \mathbf{B} \\ \mathbf{C} & \mathbf{D} \end{pmatrix}\cdot\begin{pmatrix} \boldsymbol{F}^+(z_0) \\ \boldsymbol{F}^-(z_2) \end{pmatrix} + \begin{pmatrix} \mathbf{a}\cdot\eta_0\boldsymbol{J}_S(z_1) \\ \mathbf{b}\cdot\eta_0\boldsymbol{J}_S(z_1) \end{pmatrix} \tag{5.3}$$

We proceed by finding the two-dimensional dyadics $\mathbf{A}$, $\mathbf{B}$, $\mathbf{C}$, $\mathbf{D}$, $\mathbf{a}$, and $\mathbf{b}$. These dyadics are obtained from (2.7)

$$\begin{pmatrix} \boldsymbol{E}_{xy}(z_0) \\ \eta_0\mathbf{J}\cdot\boldsymbol{H}_{xy}(z_0) \end{pmatrix} = \mathbf{S}^{-1}\cdot\begin{pmatrix} \boldsymbol{F}^+(z_0) \\ \boldsymbol{F}^-(z_0) \end{pmatrix}$$

and (5.2). We get

$$\begin{aligned} \begin{pmatrix} \boldsymbol{E}_{xy}(z_0) \\ \eta_0\mathbf{J}\cdot\boldsymbol{H}_{xy}(z_0) \end{pmatrix} =& \mathbf{S}^{-1}\cdot\begin{pmatrix} \mathbf{I}_2 & \mathbf{0} \\ -\mathbf{T}_{22}^{-1}(z_2,z_0)\cdot\mathbf{T}_{21}(z_2,z_0) & \mathbf{T}_{22}^{-1}(z_2,z_0) \end{pmatrix}\cdot\begin{pmatrix} \boldsymbol{F}^+(z_0) \\ \boldsymbol{F}^-(z_2) \end{pmatrix} \\ &+ \mathbf{S}^{-1}\cdot\begin{pmatrix} \mathbf{0} \\ -\mathbf{T}_{22}^{-1}(z_2,z_0)\cdot\mathbf{G}_{22}(z_2,z_1)\cdot\eta_0\boldsymbol{J}_S(z_1) \end{pmatrix} \end{aligned}$$

from which we identify

$$\begin{cases} \mathbf{A} = \mathbf{I}_2 - \mathbf{T}_{22}^{-1}(z_2, z_0) \cdot \mathbf{T}_{21}(z_2, z_0) = 2\mathbf{T}_{22}^{-1}(z_2, z_0) \cdot \mathbf{G}_{22}(z_2, z_0) \cdot \mathbf{W}^{-1} \\ \mathbf{B} = \mathbf{T}_{22}^{-1}(z_2, z_0) \\ \mathbf{C} = -\mathbf{W}^{-1} - \mathbf{W}^{-1} \cdot \mathbf{T}_{22}^{-1}(z_2, z_0) \cdot \mathbf{T}_{21}(z_2, z_0) = -2\mathbf{W}^{-1} \cdot \mathbf{T}_{22}^{-1}(z_2, z_0) \cdot \mathbf{G}_{21}(z_2, z_0) \\ \mathbf{D} = \mathbf{W}^{-1} \cdot \mathbf{T}_{22}^{-1}(z_2, z_0) \end{cases} \tag{5.4}$$

and

$$\begin{cases} \mathbf{a} = -\mathbf{T}_{22}^{-1}(z_2, z_0) \cdot \mathbf{G}_{22}(z_2, z_1) \\ \mathbf{b} = -\mathbf{W}^{-1} \cdot \mathbf{T}_{22}^{-1}(z_2, z_0) \cdot \mathbf{G}_{22}(z_2, z_1) \end{cases} \tag{5.5}$$

We see that the dyadics $\mathbf{A}$, $\mathbf{B}$, $\mathbf{C}$, and $\mathbf{D}$ are identical to the ones in (3.8). Moreover, the result is identical to the one found in Ref. 5. This latter statement is harder to see, and it is proven in detail in Appendix A.

In conclusion, we see that the possible singularities of the electric or the magnetic fields, $\boldsymbol{E}_{xy}(z_0)$ and $\boldsymbol{H}_{xy}(z_0)$, in (5.3) occur at $\boldsymbol{k}_t$, where $\boldsymbol{k}_t$ are determined by:

1. Possible zero eigenvalues of the two-dimensional dyadic $\mathbf{T}_{22}(z_2, z_0)$. These singularities correspond to surface waves in the entire supporting slab and are determined by the $\boldsymbol{k}_{t\text{sw}}$-value ($\hat{\boldsymbol{k}_t}$ fixed) for which $\det \mathbf{T}_{22}(z_2, z_0) = 0$. This condition is identical to the condition of surface waves in the absence of metallic screen that was investigated in Section 3.

2. Possible singularities of the surface current density $\boldsymbol{J}_S(z_1)$. These singularities depend on the shape of the metal pattern and the size of the unit cell as well as the dimensions and the material parameters of the supporting slab.

6 Periodic materials—FSS

In this section, we investigate the case when the screen at $z = z_1$ is a periodically repeated pattern, and the incident field is a plane wave incident from left with a wave vector $\boldsymbol{k}^i$. The case of incident field from the right is obtained by superposition.

We denote the unit cell by U, its area $A_U = |\boldsymbol{a} \times \boldsymbol{b}| = ab \sin\phi_0$, and the metallic parts in the unit cell by S_σ, see Figure 8. The components of $\boldsymbol{k}^i$ in the x- and y-directions are denoted by k_x^i and k_y^i, respectively, *i.e.*, $\boldsymbol{k}_t^i = \hat{\boldsymbol{x}} k_x^i + \hat{\boldsymbol{y}} k_y^i$, and the spherical angles of $\boldsymbol{k}^i$ are denoted $\theta_i \in [0, \pi/2)$ (polar angle) and $\phi_i \in [0, 2\pi)$ (azimuth angle), *i.e.*, $\boldsymbol{k}^i = k_0(\hat{\boldsymbol{x}} \sin\theta_i \cos\phi_i + \hat{\boldsymbol{y}} \sin\theta_i \sin\phi_i + \hat{\boldsymbol{z}} \cos\theta_i)$.

The Floquet wave vectors $\boldsymbol{k}_{tmn}$ are defined as

$$\boldsymbol{k}_{tmn} = 2\pi \left(-m \frac{\hat{\boldsymbol{z}} \times \boldsymbol{b}}{\hat{\boldsymbol{z}} \cdot (\boldsymbol{a} \times \boldsymbol{b})} + n \frac{\hat{\boldsymbol{z}} \times \boldsymbol{a}}{\hat{\boldsymbol{z}} \cdot (\boldsymbol{a} \times \boldsymbol{b})} \right) + \boldsymbol{k}_t^i, \qquad m, n \in \mathbb{Z} \tag{6.1}$$

Notice that $\boldsymbol{k}_{00} = \boldsymbol{k}_t^i$. For the special geometry in Figure 8, where $\boldsymbol{a} = \hat{\boldsymbol{x}} a$ and $\boldsymbol{b} = \hat{\boldsymbol{x}} b \cos\phi_0 + \hat{\boldsymbol{y}} b \sin\phi_0$, we arrive the result presented in [7], namely $\boldsymbol{k}_{tmn} = \hat{\boldsymbol{x}} \alpha_m + \hat{\boldsymbol{y}} \beta_{mn}$

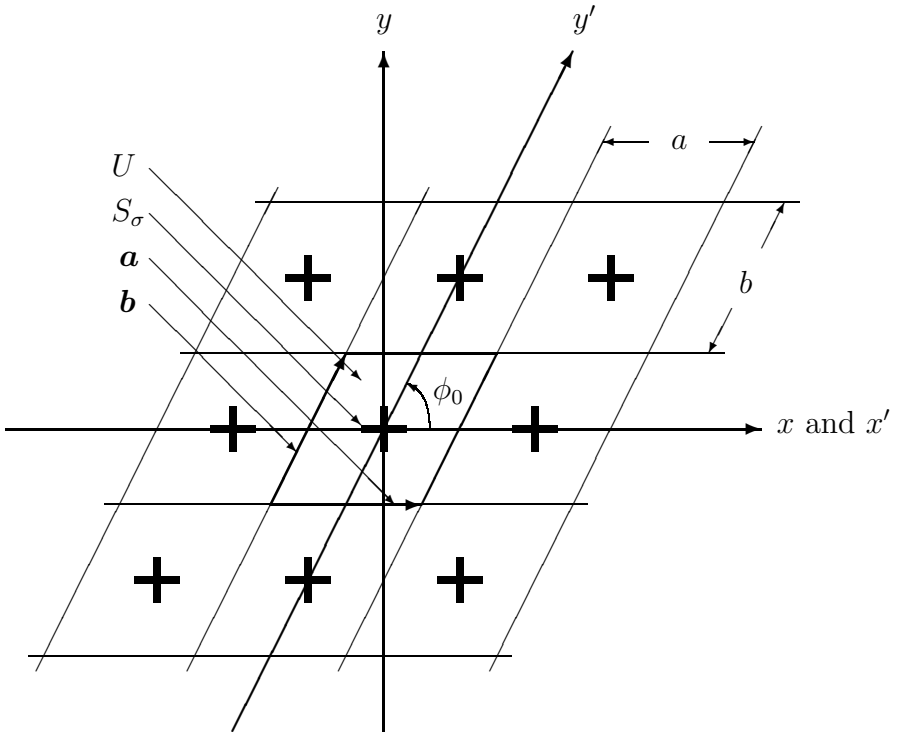

Figure 8: The unit cell U (patch case) generated by $\boldsymbol{a}$ and $\boldsymbol{b}$ with lengths $a = |\boldsymbol{a}|$ and $b = |\boldsymbol{b}|$.

with

$$\begin{cases} \alpha_m = \dfrac{2\pi m}{a} + k_x^i \\ \beta_{mn} = \dfrac{2\pi n}{b\sin\phi_0} - \dfrac{2\pi m}{a}\cot\phi_0 + k_y^i \end{cases} \qquad m, n \in \mathbb{Z}$$

The length of the Floquet vector $\boldsymbol{k}_{tmn}$ is

$$|\boldsymbol{k}_{tmn}|^2 = \left(\frac{2\pi m}{a} + k_0 \sin\theta_i \cos\phi_i\right)^2 + \left(\frac{2\pi n}{b\sin\phi_0} - \frac{2\pi m}{a}\cot\phi_0 + k_0 \sin\theta_i \sin\phi_i\right)^2$$

We also introduce the corresponding z-component of the Floquet wave vector k_{zmn}.

$$\boldsymbol{k}_{mn}^{\pm} = \boldsymbol{k}_{tmn} \pm \hat{\boldsymbol{z}} k_{zmn}, \qquad m, n \in \mathbb{Z}$$

where

$$k_{zmn} = \left(k_0^2 - |\boldsymbol{k}_{tmn}|^2\right)^{1/2} = \begin{cases} \sqrt{k_0^2 - |\boldsymbol{k}_{tmn}|^2} \text{ for } |\boldsymbol{k}_{tmn}| \le k_0 \\ \mathrm{i}\sqrt{|\boldsymbol{k}_{tmn}|^2 - k_0^2} \text{ for } |\boldsymbol{k}_{tmn}| > k_0 \end{cases}$$

Note that $k_z^i = k_{z00}$.

6.1 Onset of grating lobes

The condition for propagating grating lobes is (k_{zmn} is real)

$$|\boldsymbol{k}_{tmn}| \leq k_0, \qquad m, n \in \mathbb{Z}$$

or

$$\left(\frac{2\pi m}{k_0 a} + \sin\theta_i \cos\phi_i\right)^2 + \left(\frac{2\pi n}{k_0 b \sin\phi_0} - \frac{2\pi m}{k_0 a}\cot\phi_0 + \sin\theta_i \sin\phi_i\right)^2 \leq 1$$

This grating lobe propagates in the direction (spherical angles θ_{gr}, ϕ_{gr}) determined by

$$\begin{cases} \sin\theta_{\text{gr}} \cos\phi_{\text{gr}} = \dfrac{2\pi m}{k_0 a} + \sin\theta_i \cos\phi_i \\ \sin\theta_{\text{gr}} \sin\phi_{\text{gr}} = \dfrac{2\pi n}{k_0 b \sin\phi_0} - \dfrac{2\pi m}{k_0 a}\cot\phi_0 + \sin\theta_i \sin\phi_i \end{cases}$$

We observe that, for very high frequencies, all grating lobes radiates with a transverse wave number $\boldsymbol{k}_t$ that is identical to the transverse wave number of the direction of the incident wave $\boldsymbol{k}_t^i$.

The onset of a grating lobe is determined by the k_0 value that satisfies ($m, n \in \mathbb{Z}$)

$$\left(\frac{2\pi m}{k_0 a} + \sin\theta_i \cos\phi_i\right)^2 + \left(\frac{2\pi n}{k_0 b \sin\phi_0} - \frac{2\pi m}{k_0 a}\cot\phi_0 + \sin\theta_i \sin\phi_i\right)^2 = 1 \qquad (6.2)$$

The frequencies for the onset of the grating lobes, f_{gr}, are then determined by

$$f_{\text{gr}} = \frac{k_0 c_0}{2\pi}$$

The onset of the grating lobes are independent of the dimensions and the material parameters of the supporting slab.

The onset of the grating lobes can be visualized graphically in the u-v-plane, defined by

$$\begin{cases} u = \sin\theta \cos\phi \\ v = \sin\theta \sin\phi \end{cases}$$

The visible space ($0 \leq \theta \leq \pi$, $0 \leq \phi < 2\pi$) is the interior of the unit circle in this space and the incident direction corresponds to a point (u_i, v_i) inside the unit circle, defined by (see also Figure 9)

$$\begin{cases} u_i = -\sin\theta_i \cos\phi_i \\ v_i = -\sin\theta_i \sin\phi_i \end{cases}$$

Moreover, in the u-v-plane each Floquet mode is associated with a point (u_m, v_{mn}) defined by

$$\begin{cases} u_m = \dfrac{2\pi m}{k_0 a} \\ v_{mn} = \dfrac{2\pi n}{k_0 b \sin\phi_0} - \dfrac{2\pi m}{k_0 a}\cot\phi_0 \end{cases}$$

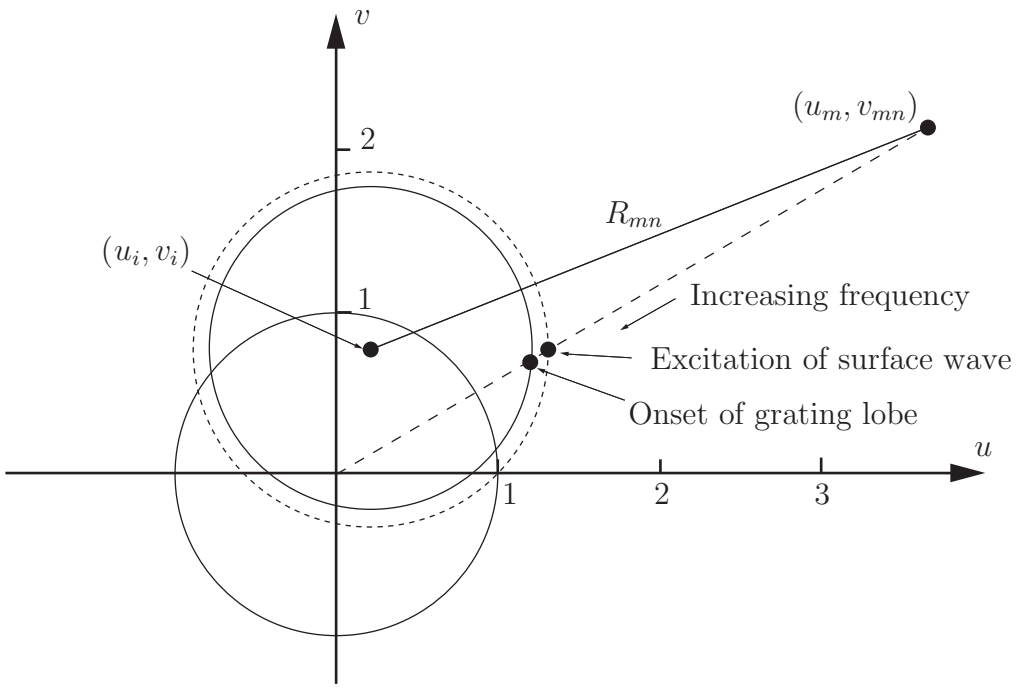

Figure 9: The geometrical interpretation of the onset of the grating lobes and the excitation of the surface waves.

Notice that, as the frequency increases (k_0 increases), this point moves along a line through the origin, see also Figure 9. With this notation, the distance R_{mn} between the point (u_m, v_{mn}) and (u_i, v_i) is

$$R_{mn} = \sqrt{(u_m - u_i)^2 + (v_{mn} - v_i)^2}$$

The onset of the grating lobe occurs at the frequency when the distance R_{mn} becomes one, *i.e.*, intersects the unit circle centered around (u_i, v_i).

6.2 Surface waves

We now address the excitation of surface waves in a periodic structure like a frequency selective structure, that is excited by an incident plane wave.

A necessary condition for the excitation of a (periodic) surface mode is

$$\boldsymbol{k}_{t\mathrm{sw}}(\hat{\boldsymbol{k}_t}) = \boldsymbol{k}_{tmn}, \qquad \text{for some index values } m, n$$

where $\boldsymbol{k}_{t\mathrm{sw}}$ are determined by the zero eigenvalues of $\mathbf{T}_{22}$ for a given k_0 ($\hat{\boldsymbol{k}_t}$ fixed), material parameters, and geometry of the slab. If this condition is not met, no excitation of the surface wave is possible. Physically, this condition means that the Floquet mode with transverse wave number $\boldsymbol{k}_{tmn}$ acts as a source of the surface wave with transverse wave number $\boldsymbol{k}_{t\mathrm{sw}}$. If the polarization of the Floquet mode and the polarization of the surface wave overlap the surface wave can be excited.

6.2.1 Isotropic material

Provided the dielectric slab is an isotropic material, the transverse wave numbers have to satisfy

$$\boldsymbol{k}_{tmn} = |\boldsymbol{k}_{t\mathrm{sw}}|\hat{\boldsymbol{e}}_{\|} = k_{t\mathrm{sw}}\hat{\boldsymbol{e}}_{\|}$$

for some m, n-value, *i.e.*,

$$\begin{cases} \dfrac{k_{t\mathrm{sw}}}{k_0}\cos\phi_{\mathrm{sw}} = \dfrac{2\pi m}{k_0 a} + \sin\theta_i\cos\phi_i \\ \dfrac{k_{t\mathrm{sw}}}{k_0}\sin\phi_{\mathrm{sw}} = \dfrac{2\pi n}{k_0 b\sin\phi_0} - \dfrac{2\pi m}{k_0 a}\cot\phi_0 + \sin\theta_i\sin\phi_i \end{cases}$$

which implies

$$\left(\frac{k_{t\mathrm{sw}}}{k_0}\right)^2 = \left(\frac{2\pi m}{k_0 a} + \sin\theta_i\cos\phi_i\right)^2 + \left(\frac{2\pi n}{k_0 b\sin\phi_0} - \frac{2\pi m}{k_0 a}\cot\phi_0 + \sin\theta_i\sin\phi_i\right)^2$$

or in the notation of Section 6.1

$$\left(\frac{k_{t\mathrm{sw}}}{k_0}\right)^2 = (u_m - u_i)^2 + (v_{mn} - v_i)^2 \tag{6.3}$$

For each value of m, n, this equation determines the frequency of excitation of a surface wave, provided the surface wave can be excited due to polarization effects. Since $k_{t\mathrm{sw}}/k_0 > 1$, see Figures 4–6, this will occur at a frequency that is smaller than the corresponding onset of the grating lobe, see Figure 9. Notice also the distinction between the onset of a surface wave and the excitation of a surface wave. These occur at two different frequencies.

6.3 Resonances in the FSS

The resonances in the periodic metallic pattern are determined by solving an integral equation. This is most conveniently done by employing the Galerkin's method [4]. In this section, we give a brief overview of the basic equations in this method for the patch case. For a more detailed description, we refer to [5].

Applying Floquet's theorem [3] to the induced surface current density at the screens, $\boldsymbol{J}_S(\boldsymbol{\rho}, z_1) = \mathbf{J}\cdot\big(\boldsymbol{H}(\boldsymbol{\rho}, z_1^+) - \boldsymbol{H}(\boldsymbol{\rho}, z_1^-)\big)$, which is non-zero on the metallic parts, S_σ, and zero elsewhere on the plane $z = z_1$, gives

$$\boldsymbol{J}_S(\boldsymbol{\rho}, z_1) = \frac{1}{A_U}\sum_{m,n=-\infty}^{\infty} \boldsymbol{J}_S|_U(\boldsymbol{k}_{tmn}, z_1)\mathrm{e}^{\mathrm{i}\boldsymbol{k}_{tmn}\cdot\boldsymbol{\rho}}, \qquad \boldsymbol{\rho}\in\mathbb{R}^2$$

where the lateral wave numbers $\boldsymbol{k}_{tmn}$ are given by equation (6.1), and the coefficient $\boldsymbol{J}_S|_U(\boldsymbol{k}_{tmn}, z_1)$ is the lateral Fourier transform of $\boldsymbol{J}_S(\boldsymbol{\rho}, z_1)$ restricted to the unit cell U and evaluated at $\boldsymbol{k}_{tmn}$, *i.e.*,

$$\boldsymbol{J}_S|_U(\boldsymbol{k}_{tmn}, z_1) = \iint_U \boldsymbol{J}_S(\boldsymbol{\rho}, z_1)\mathrm{e}^{-\mathrm{i}\boldsymbol{k}_{tmn}\cdot\boldsymbol{\rho}}dxdy$$

Notice that this quantity is identical to the Fourier coefficient of the periodic function $\boldsymbol{J}_S(\boldsymbol{\rho}, z_1)\mathrm{e}^{-\mathrm{i}\boldsymbol{k}_t^i\cdot\boldsymbol{\rho}}$. The symbol $|_U$ is used here and below to emphasize that the quantity is a lateral Fourier transform of an aperiodic quantity with support in the unit cell U and to distinguish between $\boldsymbol{J}_S(\boldsymbol{k}_t, z_1)$ and $\boldsymbol{J}_S|_U(\boldsymbol{k}_{tmn}, z_1)$. The connection between the lateral Fourier transforms of the surface current densities, $\boldsymbol{J}_S(\boldsymbol{k}_t, z_1)$, and its restriction to the unit cell, $\boldsymbol{J}_S|_U(\boldsymbol{k}_{tmn}, z_1)$, is

$$\boldsymbol{J}_S(\boldsymbol{k}_t, z_1) = \frac{4\pi^2}{A_U}\sum_{m,n=-\infty}^{\infty}\boldsymbol{J}_S|_U(\boldsymbol{k}_{tmn}, z_1)\delta(\boldsymbol{k}_t - \boldsymbol{k}_{tmn}) \tag{6.4}$$

This connection can now be used in the results in the previous sections.

Similarly, applying Floquet's theorem to the lateral electric field at the screen, $\boldsymbol{E}_{xy}(\boldsymbol{\rho}, z_1)$, yields

$$\boldsymbol{E}_{xy}(\boldsymbol{\rho}, z_1) = \frac{1}{A_U}\sum_{m,n=-\infty}^{\infty}\boldsymbol{E}_{xy}|_U(\boldsymbol{k}_{tmn}, z_1)\mathrm{e}^{\mathrm{i}\boldsymbol{k}_{tmn}\cdot\boldsymbol{\rho}}$$

where the coefficient $\boldsymbol{E}_{xy}|_U(\boldsymbol{k}_{tmn}, z_1)$ is the lateral Fourier transform of $\boldsymbol{E}_{xy}(\boldsymbol{\rho}, z_1)$ restricted to the unit cell U and evaluated at $\boldsymbol{k}_{tmn}$, *i.e.*,

$$\boldsymbol{E}_{xy}|_U(\boldsymbol{k}_{tmn}, z_1) = \iint_U \boldsymbol{E}_{xy}(\boldsymbol{\rho}, z_1)\mathrm{e}^{-\mathrm{i}\boldsymbol{k}_{tmn}\cdot\boldsymbol{\rho}}dxdy$$

Consequently, the lateral Fourier transforms of the lateral electric fields are

$$\boldsymbol{E}_{xy}(\boldsymbol{k}_t, z_1) = \frac{4\pi^2}{A_U}\sum_{m,n=-\infty}^{\infty}\boldsymbol{E}_{xy}|_U(\boldsymbol{k}_{tmn}, z_1)\delta(\boldsymbol{k}_t - \boldsymbol{k}_{tmn}) \tag{6.5}$$

The equations (6.4) and (6.5) are substituted into the relation (5.3), which is first propagated to the screen position at $z = z_1$. For an excitation from the left, we have the following relation between the transverse electric field at the screen, the surface current density on the screen, and the excitation from the left.

$$\boldsymbol{E}_{xy}|_U(\boldsymbol{k}_{mn}, z_1) = \boldsymbol{\alpha}(\boldsymbol{k}_{mn})\cdot\eta_0\boldsymbol{J}_S|_U(\boldsymbol{k}_{mn}, z_1) - A_U\boldsymbol{\beta}(\boldsymbol{k}_{00})\cdot\boldsymbol{F}^+(\boldsymbol{k}_{00}, z_0)\delta_{m0}\delta_{n0} \tag{6.6}$$

where the $\boldsymbol{\alpha}$- and $\boldsymbol{\beta}$-dyadics are combinations of the dyadics $\mathbf{A}$, $\mathbf{B}$, $\mathbf{C}$, $\mathbf{D}$, $\mathbf{a}$, and $\mathbf{b}$, defined in (5.4) and (5.5), respectively, and the propagator dyadics. See also Appendix A for additional details.

The current density $\boldsymbol{J}_S(\boldsymbol{\rho}, z_1)$ can be expanded with arbitrary precision in a pertinent complete set of entire domain or local basis functions $\boldsymbol{j}_p(\boldsymbol{\rho})$ (supported on the patches), *i.e.*,

$$\boldsymbol{J}_S(\boldsymbol{\rho}, z_1) = \sum_{p\in\chi} C_p\boldsymbol{j}_p(\boldsymbol{\rho}), \qquad \boldsymbol{\rho}\in U$$

where χ is a set of indices (countable set) and the scalars C_p are the unknown expansion coefficients. It suffices to define the basis functions $\boldsymbol{j}_p(\boldsymbol{\rho})$ in the unit cell U. The lateral Fourier transform of this expansion is

$$\boldsymbol{J}_S|_U(\boldsymbol{k}_{mn}, z_1) = \sum_{p\in\chi} C_p\boldsymbol{j}_p(\boldsymbol{k}_{mn})$$

where

$$\boldsymbol{j}_p(\boldsymbol{k}_{mn}) = \iint\limits_U \boldsymbol{j}_p(\boldsymbol{\rho}, z)\mathrm{e}^{-i\boldsymbol{k}_{mn}\cdot\boldsymbol{\rho}}dxdy, \qquad p \in \chi$$

We assume that an appropriate set of weight functions $\boldsymbol{w}_p(\boldsymbol{\rho})$ (supported on the patch) has been defined. In the Galerkin's method the functions $\boldsymbol{j}_p(\boldsymbol{\rho})$ are used. The lateral Fourier transform of the weight functions $\boldsymbol{w}_p(\boldsymbol{\rho})$ is defined as

$$\boldsymbol{w}_p(\boldsymbol{k}_{mn}) = \iint\limits_U \boldsymbol{w}_p(\boldsymbol{\rho})\mathrm{e}^{-i\boldsymbol{k}_{mn}\cdot\boldsymbol{\rho}}dxdy$$

We introduce the following identity, which follows from the boundary condition of the transverse electric field on the screen and the support of the weight functions (the two vectors in the integrand have disjoint support in the unit cell)

$$\iint\limits_U \boldsymbol{w}_p(\boldsymbol{\rho})^* \cdot \boldsymbol{E}_{xy}(\boldsymbol{\rho}, z_1)\, dx\, dy = 0, \qquad p \in \chi$$

and apply the Parseval theorem for Fourier series to this identity. This gives

$$\sum_{m,n=-\infty}^{\infty} \boldsymbol{w}_p(\boldsymbol{k}_{mn})^* \cdot \boldsymbol{E}_{xy}|_U(\boldsymbol{k}_{mn}, z_1) = 0, \qquad p \in \chi$$

in which equation (6.6) can be substituted and a system of equations for the unknown C_p is obtained. Specifically, $(p \in \chi)$

$$\sum_{m,n=-\infty}^{\infty} \boldsymbol{w}_p(\boldsymbol{k}_{mn})^* \cdot \boldsymbol{\alpha}(\boldsymbol{k}_{mn}) \cdot \eta_0 \sum_{q\in\chi} C_q \boldsymbol{j}_q(\boldsymbol{k}_{mn}) = A_U \boldsymbol{w}_p(\boldsymbol{k}_{00})^* \cdot \boldsymbol{\beta}(\boldsymbol{k}_{00}) \cdot \boldsymbol{F}^+(\boldsymbol{k}_{00}, z_0)$$

If χ is an infinite set of indices, the above equation is an infinite system of linear equations for the unknown current coefficients C_q. We assume that if this infinite system is truncated, the solution to the truncated system approximates the exact solution. An excellent treatment of the convergence properties of the Galerkin's method (and other projection methods) is found in [4]. When the linear system is truncated, it can be written as

$$\mathbf{A}\boldsymbol{C} = \boldsymbol{b}$$

where $\mathbf{A}$ is a square matrix, $\boldsymbol{C}$ is a vector containing the unknown coefficients C_q, and $\boldsymbol{b}$ is a known vector. Specifically, the matrix elements are

$$A_{pq} = \eta_0 \sum_{m,n=-\infty}^{\infty} \boldsymbol{w}_p(\boldsymbol{k}_{mn})^* \cdot \boldsymbol{\alpha}(\boldsymbol{k}_{mn}) \cdot \boldsymbol{j}_q(\boldsymbol{k}_{mn}) \qquad p, q \in \chi$$

and the right-hand entries are

$$b_p = A_U \boldsymbol{w}_p(\boldsymbol{k}_{00})^* \cdot \boldsymbol{\beta}(\boldsymbol{k}_{00}) \cdot \boldsymbol{F}^+(\boldsymbol{k}_{00}, z_0), \qquad p \in \chi$$

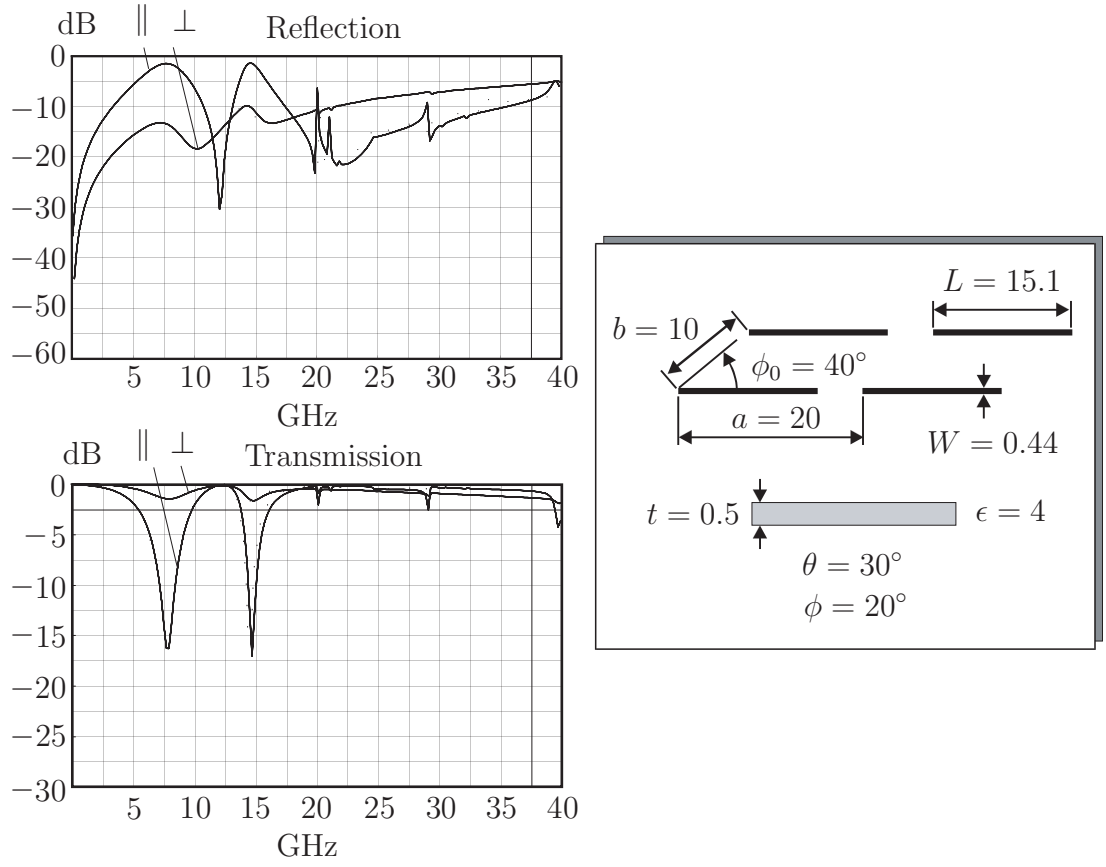

Figure 10: The reflection and transmission coefficients, *i.e.*, the radiated power in the $\boldsymbol{k}_{t00}$ direction, for a skewed array of dipoles in the parallel (TE) and the perpendicular (TM) polarizations. The onset of the two first grating lobes occurs at 21.27 GHz ($m = -2$, $n = -1$) and 22.13 GHz ($m = -1$, $n = 0$), and the onset of the first non-zero surface wave (TE_1) occurs at 173 GHz. In Figure 11, the frequency interval between 19–24 GHz is shown in detail.

7 Numerical illustrations

Three different types of resonances can occur in the reflection and transmission data for a FSS as a function of frequency. These resonance effects have similarities with the type of phenomena (scan blindness) that occur in phased arrays of printed dipoles [8]. These types of resonances are:

1. Possible zero eigenvalues of the two-dimensional dyadic $\mathbf{T}_{22}(z_2, z_0)$. For a lossy slab these are in general complex-valued. These singularities correspond to surface waves in the entire supporting slab and are determined by the $\boldsymbol{k}_{t_{\mathrm{sw}}}$-values for which $\det \mathbf{T}_{22}(z_2, z_0) = 0$ ($\hat{\boldsymbol{k}}_{\boldsymbol{t}}$ fixed). Notice that this type of resonance is independent of the FSS and depends only on the material parameters and the dimensions of the supporting slab.

2. Possible resonances of the surface current density $\boldsymbol{J}_S(z_1)$. This type of reso-

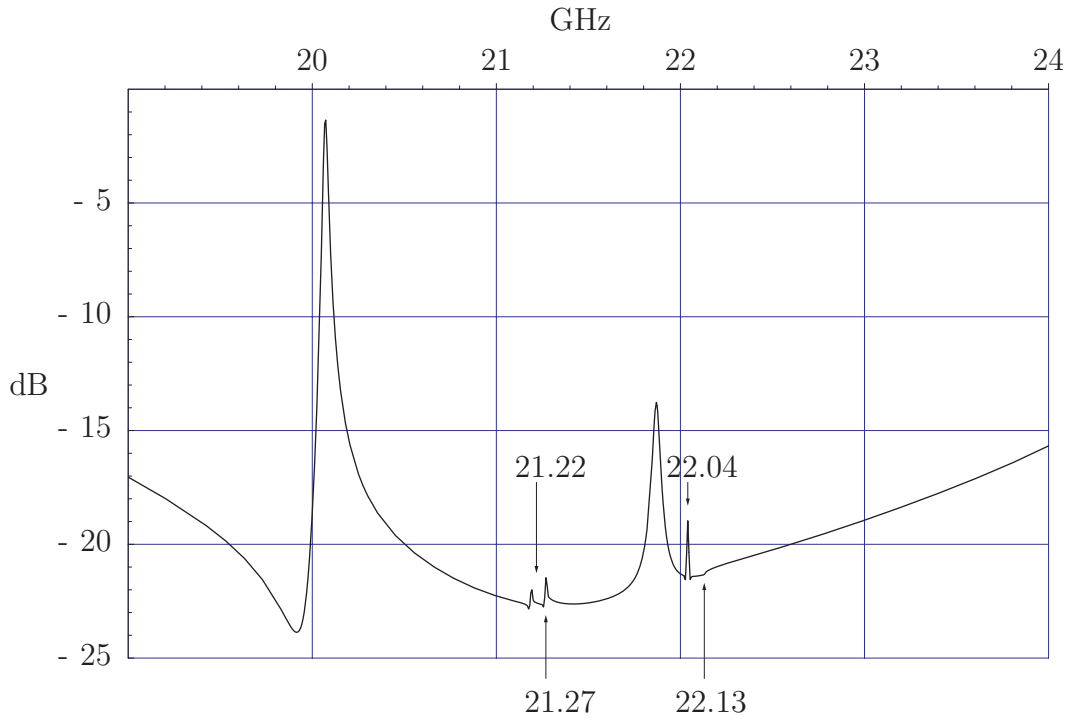

Figure 11: The reflection coefficient for a skewed array of dipoles in the parallel (TM) polarization. The geometry of the FSS and the supporting slab is given in Figure 10. The onset of the two first grating lobes occur at 21.27 GHz ($m = -2$, $n = -1$) and 22.13 GHz ($m = -1$, $n = 0$).

nance depends on the FSS pattern, the material parameters, and the dimensions of the supporting slab.

3. The onset of a grating lobe initiates a disturbance in the transmission data. Notice that this type of resonance (disturbance) is independent the material parameters and the dimensions of the supporting slab, and depends only on the size and shape of the unit cell U.

We illustrate the occurrence of these resonances in a series of examples. In the first example, the first non-zero surface wave (TE_1) occurs at a frequency that is much larger than the onset of the first grating lobe. The geometry and the reflection and transmission data are shown in Figure 10. The onset of the two first grating lobes occurs at 21.27 GHz ($m = -2$, $n = -1$) and 22.13 GHz ($m = -1$, $n = 0$), and the onset of the first non-zero surface wave occurs at 173 GHz (TE_1), which is far outside the frequency ranged in the figure. The resonance behavior in the frequency range 19–24 GHz is shown in detail in Figure 11. We notice the occurrence of two pairs of resonances (one is very weak), which correspond to the excitation of a surface wave, satisfying (6.3), and the onset of the grating lobes, satisfying (6.2). The excitation of the surface mode TM_0 is made first at a frequency of 21.22 GHz by the grating lobe with indices $(m, n) = (-2, -1)$, and a second excitation of the

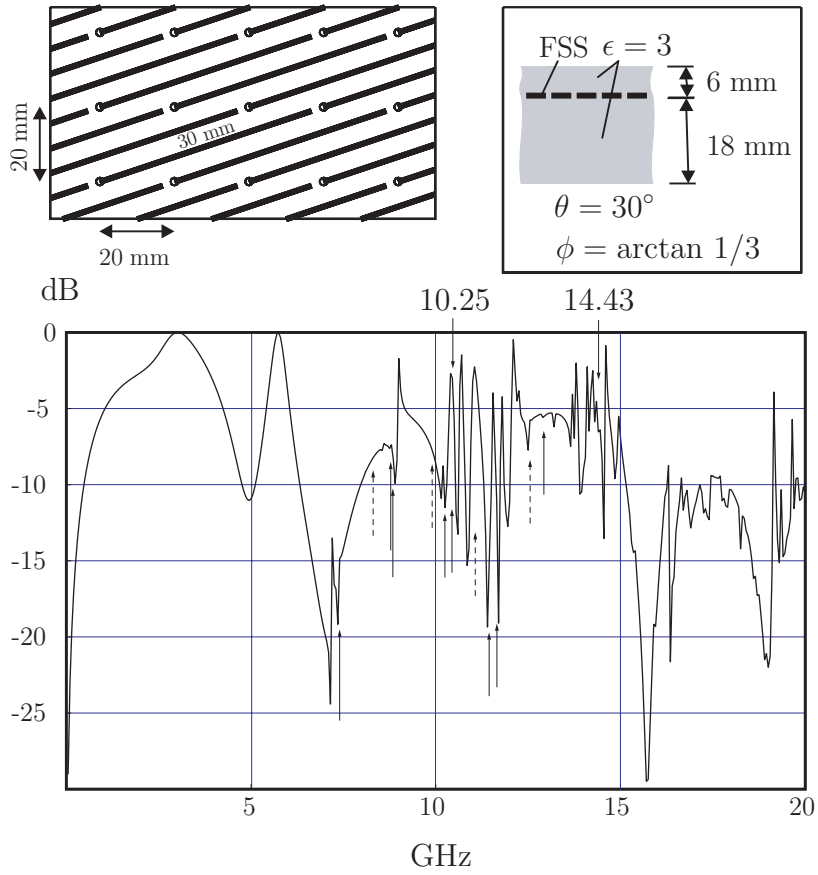

Figure 12: The reflection coefficient for the parallel polarization (TM-case) for an array of gangbuster elements (type 3) that supports several surface waves in the frequency interval depicted. The onset of the first two grating lobes occurs at 10.25 GHz ($m = -1$, $n = 0$) and 14.43 GHz ($m = 0$, $n = -1$). The excitation of the surface modes occurs at 7.37, 8.82, 10,23, 11.63 GHz for the TM_0-modes, see also Figure 13, and for the TM_1-modes the excitation is at 8.76, 10.40, 11.43, 12.91 GHz, see also Figure 14. The excitation of the TM_1-modes are marked with solid arrows. The excitation of the surface modes occurs at 8.27, 9.88, 11.05, 12.54 GHz for the TE_1-modes, which are marked with dashed arrows, see also Figure 15.

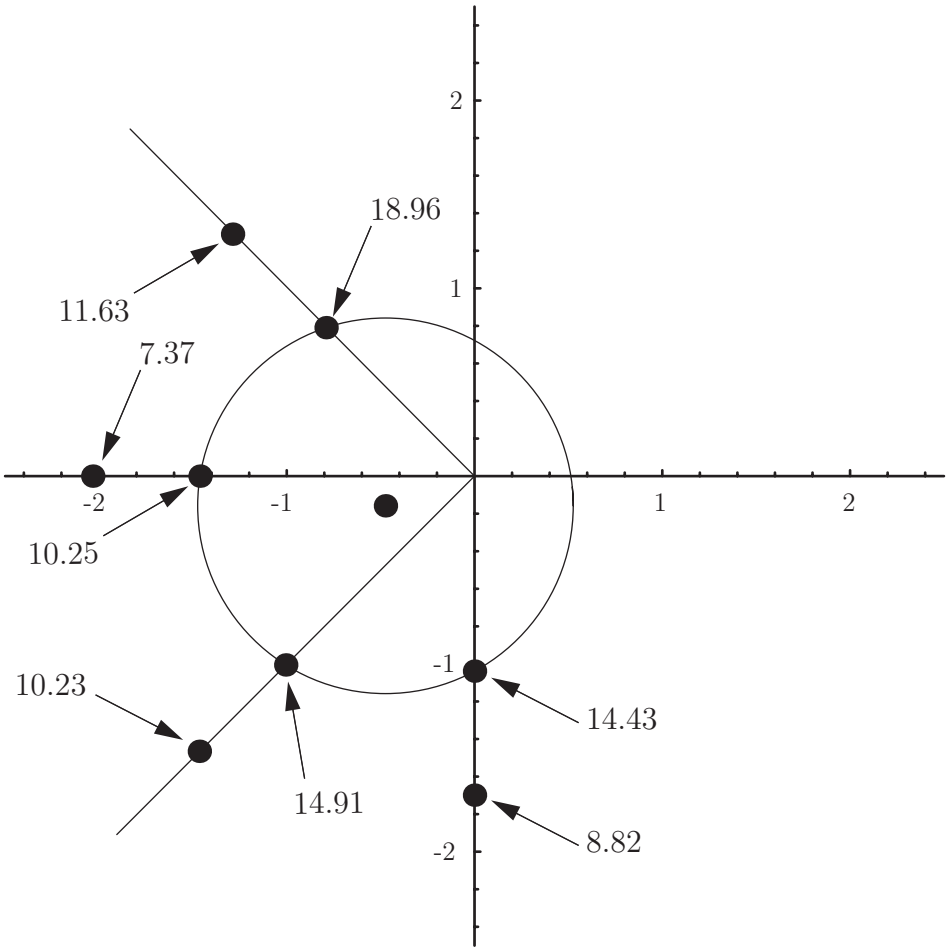

Figure 13: The geometrical interpretation of the onset of the grating lobes and the excitation of the surface waves for a TM_0-mode in Figure 12. The solid dot in the center of the circle marks the direction of the incident field, *i.e.*, (u_i, v_i).

same surface mode is made at a frequency of 22.04 GHz by the grating lobe with indices $(m, n) = (-1, 0)$.

The second example is shown in Figures 12–16. The slab is in this example has a much thicker substrate, and, therefore, the surface wave are generated at a much lower frequency. In fact, lower than the frequency of the first grating lobe. The onset of the first two grating lobes occurs at 10.25 GHz ($m = -1$, $n = 0$) and 14.43 GHz ($m = 0$, $n = -1$), and the onset of the first two non-zero surface wave occurs at 4.42 GHz (TE_1) and 8.83 GHz (TM_1). The azimuthal direction of the incident wave coincides with the direction of the dipoles. This implies that only excitations of surface waves are possible in the TM-case, see Figure 12. The situation is here very complex and several Floquet modes and surface waves interact in a complex way. The excitation of the surface mode TM_0 is made first at a frequency of 7.37 GHz by the grating lobe with indices $(m, n) = (-1, 0)$, and a second excitation of the same surface mode is made at a frequency of 8.82 GHz by the grating lobe with

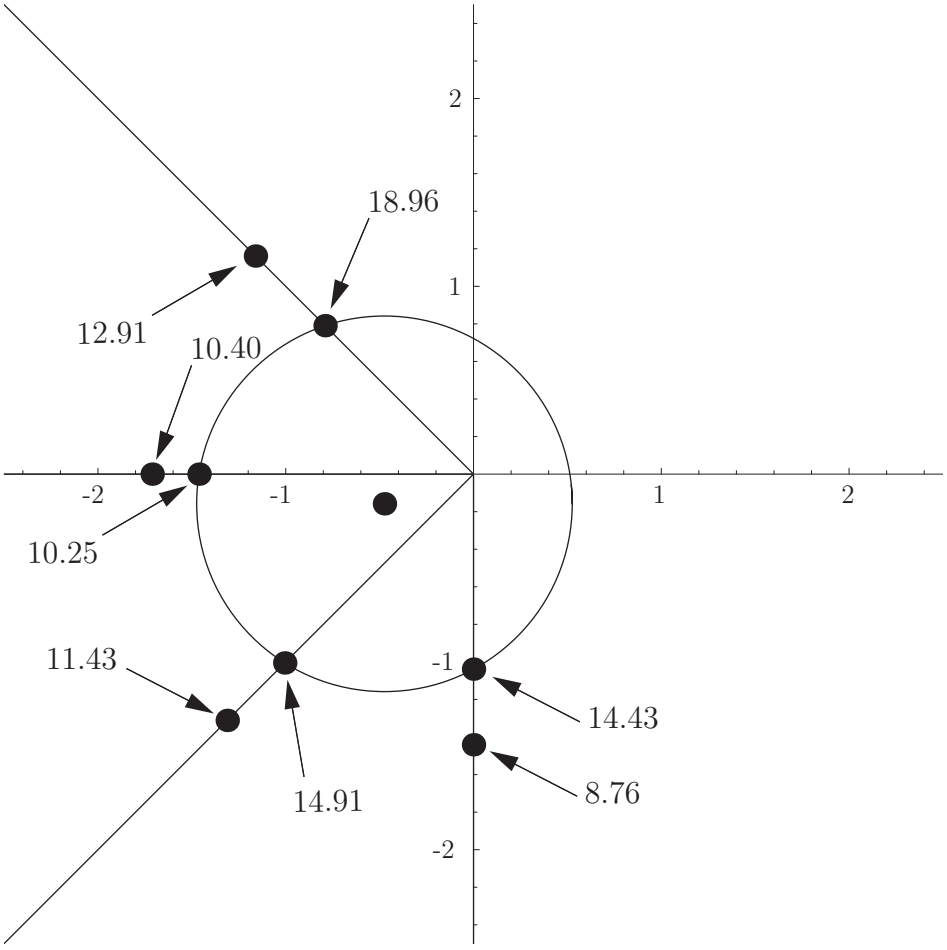

Figure 14: The geometrical interpretation of the onset of the grating lobes and the excitation of the surface waves for a TM_1-mode in Figure 12. The solid dot in the center of the circle marks the direction of the incident field, *i.e.*, (u_i, v_i).

indices $(m, n) = (0, -1)$. Several other excitations occur and the situation becomes extremely complex at frequencies above 10 GHz. In the perpendicular polarization (TE-case), no surface waves are excited, see Figure 16, due to the polarization of the incident wave. The reflection pattern is now as of a simple, homogenous dielectric slab without FSS.

8 Conclusions

We have seen that in the absence of a metal screen, *i.e.*, a pure dielectric slab, no surface waves can be excited by an incident plane wave. An incident source with a wider plane wave spectrum is needed to excite the surface wave. In the presence of a FSS, this condition is met, if the Floquet wave vector coincides with the transverse

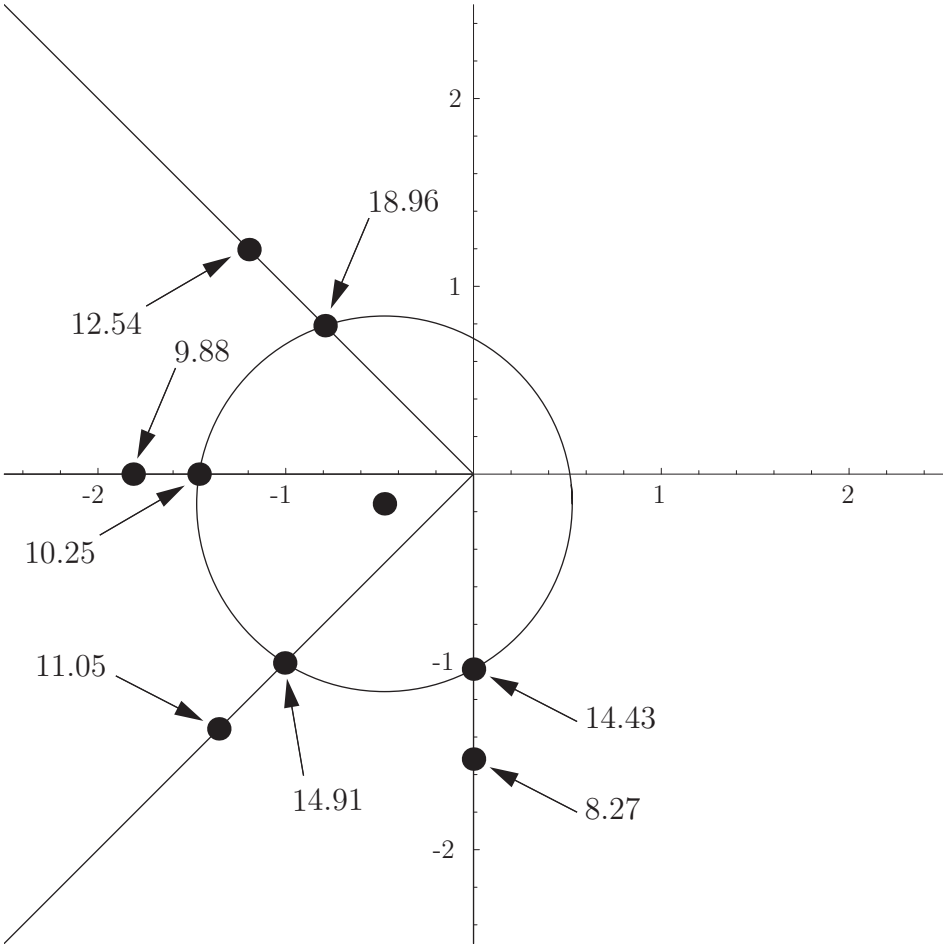

Figure 15: The geometrical interpretation of the onset of the grating lobes and the excitation of the surface waves for a TE_1-mode in Figure 12. The solid dot in the center of the circle marks the direction of the incident field, *i.e.*, (u_i, v_i).

wave vector of the surface wave, *i.e.*,

$$\boldsymbol{k}_{t\mathrm{sw}}(\hat{\boldsymbol{k}_t}) = \boldsymbol{k}_{tmn}$$

for some index values m and n. In practice, the FSS is not infinite in its extent and the spectrum is continuous instead of discrete, so this condition is relaxed. Losses in the material also weakens the effect of surface waves. We can also conclude that the presence of surface waves below the frequencies of the onset of the grating lobes is devastating for the radome construction, and the importance of densely packed FSS elements, as well as keeping the substrate thin, is vital for a successful construction.

9 Acknowledgements

The work reported in this paper is supported by a grant from the Defense Materiel Administration (FMV), which is gratefully acknowledged. The author likes to ac-

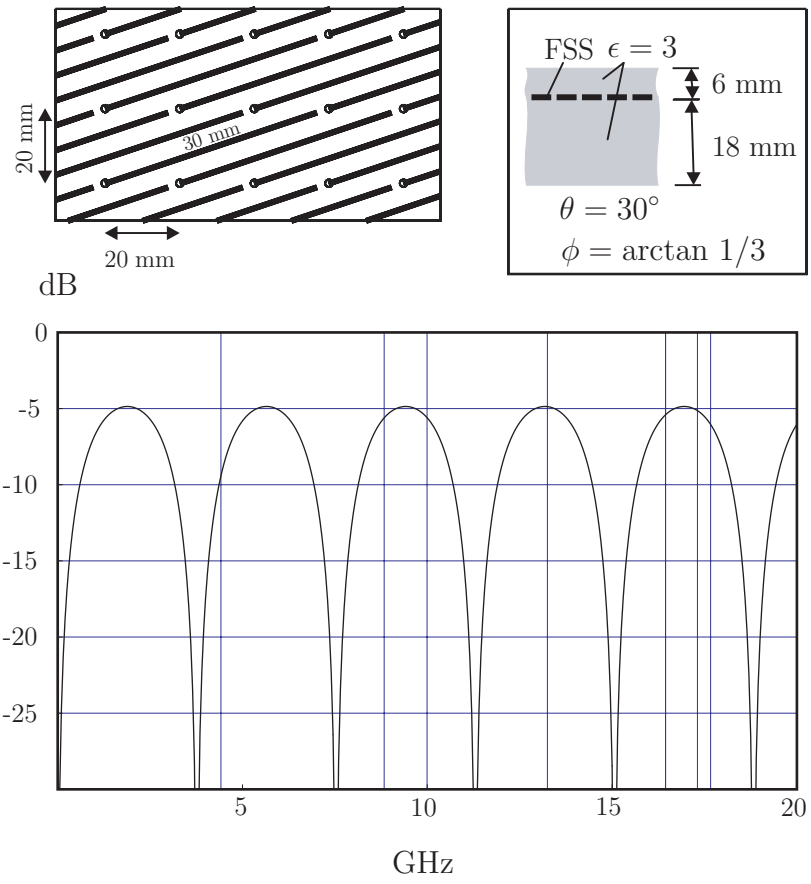

Figure 16: The reflection coefficient for the perpendicular polarization (TE-case) for an array of gangbuster elements (type 3) that supports several surface waves in the frequency interval depicted. The onset of the first two grating lobes occurs at 10.25 GHz ($m = -1$, $n = 0$) and 14.43 GHz ($m = 0$, $n = -1$), and the onset of the first two non-zero surface wave (TE_1 and TM_1) occurs at 4.42 GHz and 8.83 GHz, respectively. Note that the surface waves are not excited in this case.

knowledge Sören Poulsen, Applied Composites AB, for providing the reflection and transmission results presented in Figures 10–16.

Appendix A Comparison with TEAT-7099

Our aim in this appendix is to find a relation between the electric field at the screen and the surface current density on the screen, *i.e.*,

$$\boldsymbol{E}_{xy}(z_1) = \boldsymbol{\alpha} \cdot \boldsymbol{F}^{+}(z_0) + \boldsymbol{\beta} \cdot \boldsymbol{F}^{-}(z_2) + \boldsymbol{\gamma} \cdot \eta_0 \boldsymbol{J}_S(z_1)$$

and we like to identify the two-dimension dyadics $\boldsymbol{\alpha}$, $\boldsymbol{\beta}$, and $\boldsymbol{\gamma}$ and to compare the result with the corresponding result in [5], which is repeated in Appendix A.1 for convenience.

To accomplish this, we propagate the field from the edge, $z = z_0$, to the screen, $z = z_1$, *i.e.*,

$$\boldsymbol{E}_{xy}(z_1) = \mathbf{P}_{11}(z_1, z_0) \cdot \boldsymbol{E}_{xy}(z_0) + \mathbf{P}_{12}(z_1, z_0) \cdot \eta_0 \mathbf{J} \cdot \boldsymbol{H}_{xy}(z_0)$$

Now using (5.3) we identify

$$\begin{cases} \boldsymbol{\alpha} = \mathbf{P}_{11}(z_1, z_0) \cdot \mathbf{A} + \mathbf{P}_{12}(z_1, z_0) \cdot \mathbf{C} \\ \boldsymbol{\beta} = \mathbf{P}_{11}(z_1, z_0) \cdot \mathbf{B} + \mathbf{P}_{12}(z_1, z_0) \cdot \mathbf{D} \\ \boldsymbol{\gamma} = \mathbf{P}_{11}(z_1, z_0) \cdot \boldsymbol{a} + \mathbf{P}_{12}(z_1, z_0) \cdot \boldsymbol{b} \end{cases}$$

which we, using (5.4) and (5.5), rewrite as

$$\begin{cases} \boldsymbol{\alpha} = \mathbf{P}_{11}(z_1, z_0) - \mathbf{P}_{12}(z_1, z_0) \cdot \mathbf{W}^{-1} \\ \qquad - \left(\mathbf{P}_{11}(z_1, z_0) + \mathbf{P}_{12}(z_1, z_0) \cdot \mathbf{W}^{-1}\right) \cdot \mathbf{T}_{22}^{-1}(z_2, z_0) \cdot \mathbf{T}_{21}(z_2, z_0) \\ \boldsymbol{\beta} = \left(\mathbf{P}_{11}(z_1, z_0) + \mathbf{P}_{12}(z_1, z_0) \cdot \mathbf{W}^{-1}\right) \cdot \mathbf{T}_{22}^{-1}(z_2, z_0) \\ \boldsymbol{\gamma} = -\left(\mathbf{P}_{11}(z_1, z_0) + \mathbf{P}_{12}(z_1, z_0) \cdot \mathbf{W}^{-1}\right) \cdot \mathbf{T}_{22}^{-1}(z_2, z_0) \cdot \mathbf{G}_{22}(z_2, z_1) \end{cases}$$

We now prove that these dyadics are equivalent to the results obtained in [5].

Use (3.4) and (3.5) to get

$$\mathbf{G}(z_2, z_0) = \mathbf{G}(z_2, z_1) \cdot \mathbf{P}(z_1, z_0)$$

$$\mathbf{T}(z_2, z_0) = \mathbf{G}(z_2, z_1) \cdot (\mathbf{G}(z_0, z_1))^{-1}$$

It is convenient to introduce a special symbol to the dyadic $\mathbf{G}(z_0, z_1)$ and its inverse.

$$\begin{cases} \mathbf{g} = \mathbf{G}(z_0, z_1) \\ \mathbf{h} = (\mathbf{G}(z_0, z_1))^{-1} \end{cases}$$

In this notation, we get

$$\mathbf{T}_{22}(z_2, z_0) = \mathbf{G}_{21}(z_2, z_1) \cdot \mathbf{h}_{12} + \mathbf{G}_{22}(z_2, z_1) \cdot \mathbf{h}_{22}$$

which we rewrite as, see Appendix B

$$\begin{aligned}\mathbf{T}_{22}(z_2,z_0) =& \left(-\mathbf{G}_{21}(z_2,z_1)+\mathbf{G}_{22}(z_2,z_1)\cdot\mathbf{g}_{12}^{-1}\cdot\mathbf{g}_{11}\right)\cdot\left(\mathbf{g}_{22}\cdot\mathbf{g}_{12}^{-1}\cdot\mathbf{g}_{11}-\mathbf{g}_{21}\right)^{-1}\\ =&\mathbf{G}_{22}(z_2,z_1)\cdot\left(-\mathbf{G}_{22}^{-1}(z_2,z_1)\cdot\mathbf{G}_{21}(z_2,z_1)+\mathbf{g}_{12}^{-1}\cdot\mathbf{g}_{11}\right)\\ &\cdot\left(\mathbf{g}_{22}\cdot\mathbf{g}_{12}^{-1}\cdot\mathbf{g}_{11}-\mathbf{g}_{21}\right)^{-1}\end{aligned}$$

We get

$$\mathbf{T}_{22}(z_2,z_0)=\mathbf{G}_{22}(z_2,z_1)\cdot\mathbf{A}_{11}\cdot\left(\mathbf{g}_{22}\cdot\mathbf{g}_{12}^{-1}\cdot\mathbf{g}_{11}-\mathbf{g}_{21}\right)^{-1}$$

where

$$\mathbf{A}_{11}=-\mathbf{G}_{22}^{-1}(z_2,z_1)\cdot\mathbf{G}_{21}(z_2,z_1)+\mathbf{g}_{12}^{-1}\cdot\mathbf{g}_{11}$$

and, see Appendix B

$$\begin{aligned}\mathbf{T}_{22}^{-1}(z_2,z_0) &= \left(\mathbf{g}_{22}\cdot\mathbf{g}_{12}^{-1}\cdot\mathbf{g}_{11}-\mathbf{g}_{21}\right)\cdot\mathbf{A}_{11}^{-1}\cdot\mathbf{G}_{22}^{-1}(z_2,z_1)\\ &= -\left(\mathbf{h}_{12}\right)^{-1}\cdot\mathbf{A}_{11}^{-1}\cdot\mathbf{G}_{22}^{-1}(z_2,z_1)\end{aligned}$$

We therefore get

$$\boldsymbol{\gamma}=\left(\mathbf{P}_{11}(z_1,z_0)+\mathbf{P}_{12}(z_1,z_0)\cdot\mathbf{W}^{-1}\right)\cdot\left(\mathbf{h}_{12}\right)^{-1}\cdot\mathbf{A}_{11}^{-1}$$

The factor

$$\mathbf{P}_{11}(z_1,z_0)+\mathbf{P}_{12}(z_1,z_0)\cdot\mathbf{W}^{-1}=\left(\mathbf{P}(z_1,z_0)\cdot\mathbf{S}^{-1}\right)_{12}=\left(\left(\mathbf{S}\cdot\mathbf{P}(z_0,z_1)\right)^{-1}\right)_{12}=\mathbf{h}_{12}$$

Thus

$$\boldsymbol{\gamma}=\mathbf{A}_{11}^{-1}$$

which is identical to the result in [5].

Similarly, we get

$$\boldsymbol{\beta}=-\boldsymbol{\gamma}\cdot\mathbf{G}_{22}^{-1}(z_2,z_1)=-\mathbf{A}_{11}^{-1}\cdot\mathbf{G}_{22}^{-1}(z_2,z_1)$$

which also is identical to the result in [5].

The last dyadic is different. We have

$$\begin{aligned}\boldsymbol{\alpha} =&\mathbf{P}_{11}(z_1,z_0)-\mathbf{P}_{12}(z_1,z_0)\cdot\mathbf{W}^{-1}\\ &-\left(\mathbf{P}_{11}(z_1,z_0)+\mathbf{P}_{12}(z_1,z_0)\cdot\mathbf{W}^{-1}\right)\cdot\mathbf{T}_{22}^{-1}(z_2,z_0)\cdot\mathbf{T}_{21}(z_2,z_0)\end{aligned}$$

From above, we have

$$\mathbf{T}_{22}^{-1}(z_2,z_0)=-\left(\mathbf{h}_{12}\right)^{-1}\cdot\mathbf{A}_{11}^{-1}\cdot\mathbf{G}_{22}^{-1}(z_2,z_1)$$

and

$$\mathbf{P}_{11}(z_1,z_0)+\mathbf{P}_{12}(z_1,z_0)\cdot\mathbf{W}^{-1}=\mathbf{h}_{12}$$

Similarly, we get

$$\mathbf{P}_{11}(z_1,z_0)-\mathbf{P}_{12}(z_1,z_0)\cdot\mathbf{W}^{-1}=\mathbf{h}_{11}$$

This implies

$$\boldsymbol{\alpha} = \mathbf{h}_{11} + \mathbf{A}_{11}^{-1} \cdot \mathbf{G}_{22}^{-1}(z_2, z_1) \cdot \mathbf{T}_{21}(z_2, z_0)$$

Now use

$$\mathbf{T}_{21}(z_2, z_0) = \mathbf{G}_{21}(z_2, z_1) \cdot \mathbf{h}_{11} + \mathbf{G}_{22}(z_2, z_1) \cdot \mathbf{h}_{21}$$

which we rewrite as, see Appendix B

$$\mathbf{T}_{21}(z_2, z_0) = \big(\mathbf{G}_{21}(z_2, z_1) \cdot \mathbf{g}_{21}^{-1} \cdot \mathbf{g}_{22} - \mathbf{G}_{22}(z_2, z_1)\big) \cdot \big(\mathbf{g}_{11} \cdot \mathbf{g}_{21}^{-1} \cdot \mathbf{g}_{22} - \mathbf{g}_{12}\big)^{-1}$$

and

$$\begin{aligned}
\boldsymbol{\alpha} &= \big\{\mathbf{g}_{21}^{-1} \cdot \mathbf{g}_{22} + \mathbf{A}_{11}^{-1} \cdot \mathbf{G}_{22}^{-1}(z_2, z_1) \cdot \big(\mathbf{G}_{21}(z_2, z_1) \cdot \mathbf{g}_{21}^{-1} \cdot \mathbf{g}_{22} - \mathbf{G}_{22}(z_2, z_1)\big)\big\} \\
&\quad \cdot \big(\mathbf{g}_{11} \cdot \mathbf{g}_{21}^{-1} \cdot \mathbf{g}_{22} - \mathbf{g}_{12}\big)^{-1} \\
&= \big\{\mathbf{g}_{21}^{-1} \cdot \mathbf{g}_{22} + \mathbf{A}_{11}^{-1} \cdot \big(\mathbf{G}_{22}^{-1}(z_2, z_1) \cdot \mathbf{G}_{21}(z_2, z_1) - \mathbf{g}_{22}^{-1} \cdot \mathbf{g}_{21}\big) \cdot \mathbf{g}_{21}^{-1} \cdot \mathbf{g}_{22}\big\} \\
&\quad \cdot \mathbf{g}_{22}^{-1} \cdot \big(\mathbf{g}_{12}^{-1} \cdot \mathbf{g}_{11} \cdot \mathbf{g}_{21}^{-1} - \mathbf{g}_{22}^{-1}\big)^{-1} \cdot \mathbf{g}_{12}^{-1}
\end{aligned}$$

We simplify further

$$\begin{aligned}
\boldsymbol{\alpha} &= \big\{\mathbf{I}_2 + \mathbf{A}_{11}^{-1} \cdot \big(\mathbf{G}_{22}^{-1}(z_2, z_1) \cdot \mathbf{G}_{21}(z_2, z_1) - \mathbf{g}_{22}^{-1} \cdot \mathbf{g}_{21}\big)\big\} \\
&\quad \cdot \big(\mathbf{g}_{12}^{-1} \cdot \mathbf{g}_{11} - \mathbf{g}_{22}^{-1} \cdot \mathbf{g}_{21}\big)^{-1} \cdot \mathbf{g}_{12}^{-1} \\
&= \big\{\mathbf{I}_2 + \mathbf{A}_{11}^{-1} \cdot \big(-\mathbf{A}_{11} - \mathbf{g}_{22}^{-1} \cdot \mathbf{g}_{21} + \mathbf{g}_{12}^{-1} \cdot \mathbf{g}_{11}\big)\big\} \\
&\quad \cdot \big(\mathbf{g}_{12}^{-1} \cdot \mathbf{g}_{11} - \mathbf{g}_{22}^{-1} \cdot \mathbf{g}_{21}\big)^{-1} \cdot \mathbf{g}_{12}^{-1} \\
&= -\mathbf{A}_{11}^{-1} \cdot \big(\mathbf{g}_{22}^{-1} \cdot \mathbf{g}_{21} - \mathbf{g}_{12}^{-1} \cdot \mathbf{g}_{11}\big) \cdot \big(\mathbf{g}_{12}^{-1} \cdot \mathbf{g}_{11} - \mathbf{g}_{22}^{-1} \cdot \mathbf{g}_{21}\big)^{-1} \cdot \mathbf{g}_{12}^{-1}
\end{aligned}$$

The final result is

$$\boldsymbol{\alpha} = \mathbf{A}_{11}^{-1} \cdot \mathbf{G}_{12}^{-1}(z_0, z_1)$$

which completes the proof of equivalence between the results obtained in this paper and the results of [5].

A.1 The results in TEAT-7099

From [5], we get

$$\eta_0 \boldsymbol{J}_S(\boldsymbol{k}_t, z_1) = \mathbf{A}_{11}(\boldsymbol{k}_t) \cdot \boldsymbol{E}_{xy}(\boldsymbol{k}_t, z_1) + \mathbf{A}_{10}(\boldsymbol{k}_t) \cdot \boldsymbol{F}^{+}(\boldsymbol{k}_t, z_0) + \mathbf{A}_{12}(\boldsymbol{k}_t) \cdot \boldsymbol{F}^{-}(\boldsymbol{k}_t, z_2)$$

where

$$\begin{cases}
\mathbf{A}_{11} = -\mathbf{G}_{22}^{-1}(z_2, z_1) \cdot \mathbf{G}_{21}(z_2, z_1) + \mathbf{G}_{12}^{-1}(z_0, z_1) \cdot \mathbf{G}_{11}(z_0, z_1) \\
\mathbf{A}_{12} = \mathbf{G}_{22}^{-1}(z_2, z_1) \\
\boldsymbol{A}_{10} = -\mathbf{G}_{12}^{-1}(z_0, z_1)
\end{cases}$$

$$\boldsymbol{E}_{xy}(\boldsymbol{k}_t, z_1) = \mathbf{B}_{11}(\boldsymbol{k}_t) \cdot \eta_0 \boldsymbol{J}_S(\boldsymbol{k}_t, z_1) - \mathbf{B}_{10}(\boldsymbol{k}_t) \cdot \boldsymbol{F}^{+}(\boldsymbol{k}_t, z_0) - \mathbf{B}_{12}(\boldsymbol{k}_t) \cdot \boldsymbol{F}^{-}(\boldsymbol{k}_t, z_2)$$

where

$$\begin{cases}
\mathbf{B}_{11} = \mathbf{A}_{11}^{-1} \\
\mathbf{B}_{10} = \mathbf{B}_{11} \cdot \mathbf{A}_{10} \\
\mathbf{B}_{12} = \mathbf{B}_{11} \cdot \mathbf{A}_{12}
\end{cases}$$

Possible surface modes:

$$\begin{cases} \mathbf{G}_{12}(z_0, z_1) = \mathbf{0} \\ \mathbf{G}_{12}(z_2, z_1) = \mathbf{0} \end{cases}$$

Appendix B Inverse of four-dimensional dyadic

Let

$$\mathbf{P} = \begin{pmatrix} \mathbf{A}_{11} & \mathbf{A}_{12} \\ \mathbf{A}_{21} & \mathbf{A}_{22} \end{pmatrix}$$

be a four-dimensional dyadic expressed in terms of four two-dimensional dyadics $\mathbf{A}_{ij}$, $i, j = 1, 2$. Denote the inverse of $\mathbf{P}$ as

$$\mathbf{P}^{-1} = \begin{pmatrix} \mathbf{B}_{11} & \mathbf{B}_{12} \\ \mathbf{B}_{21} & \mathbf{B}_{22} \end{pmatrix}$$

We get

$$\begin{cases} \mathbf{A}_{11} \cdot \mathbf{B}_{11} + \mathbf{A}_{12} \cdot \mathbf{B}_{21} = \mathbf{I}_2 \\ \mathbf{A}_{21} \cdot \mathbf{B}_{11} + \mathbf{A}_{22} \cdot \mathbf{B}_{21} = \mathbf{0} \end{cases} \qquad \begin{cases} \mathbf{A}_{11} \cdot \mathbf{B}_{12} + \mathbf{A}_{12} \cdot \mathbf{B}_{22} = \mathbf{0} \\ \mathbf{A}_{21} \cdot \mathbf{B}_{12} + \mathbf{A}_{22} \cdot \mathbf{B}_{22} = \mathbf{I}_2 \end{cases}$$

with solutions

$$\begin{cases} \mathbf{B}_{11} = \mathbf{A}_{21}^{-1} \cdot \mathbf{A}_{22} \cdot \left(\mathbf{A}_{11} \cdot \mathbf{A}_{21}^{-1} \cdot \mathbf{A}_{22} - \mathbf{A}_{12} \right)^{-1} \\ \mathbf{B}_{12} = -\left(\mathbf{A}_{22} \cdot \mathbf{A}_{12}^{-1} \cdot \mathbf{A}_{11} - \mathbf{A}_{21} \right)^{-1} \\ \mathbf{B}_{21} = -\left(\mathbf{A}_{11} \cdot \mathbf{A}_{21}^{-1} \cdot \mathbf{A}_{22} - \mathbf{A}_{12} \right)^{-1} \\ \mathbf{B}_{22} = \mathbf{A}_{12}^{-1} \cdot \mathbf{A}_{11} \cdot \left(\mathbf{A}_{22} \cdot \mathbf{A}_{12}^{-1} \cdot \mathbf{A}_{11} - \mathbf{A}_{21} \right)^{-1} \end{cases}$$

Appendix C Singular matrices

Assume that the n-dimensional dyadic $\mathbf{A}(k)$ depends analytically on a parameter k in a neighborhood to $k = k_\mathrm{s}$. The singular value decomposition of the matrix is [2]

$$\mathbf{A}(k) = \mathbf{U}(k) \cdot \mathbf{D}(k) \cdot \mathbf{V}^\dagger(k)$$

where $\mathbf{U}(k)$ and $\mathbf{V}(k)$ are unitary n-dimensional dyadics and $\mathbf{D}(k)$ is a diagonal dyadic with the singular values $\sigma_m(k)$ as entries in the diagonal. These dyadics depend analytically on a parameter k in a neighborhood to $k = k_\mathrm{s}$. The inverse therefore is

$$\mathbf{A}^{-1}(k) = \mathbf{V}(k) \cdot \mathbf{D}^{-1}(k) \cdot \mathbf{U}^\dagger(k)$$

If the singular values $\sigma_m(k)$ have a power series expansion

$$\sigma_m(k) = \sigma_m(k_\mathrm{s}) + \sigma'_m(k_\mathrm{s})(k - k_\mathrm{s}) + \ldots, \qquad m = 1, \ldots, n$$

in a neighborhood to $k = k_\mathrm{s}$, and where both $\{\sigma_m(k_\mathrm{s}), \sigma'_m(k_\mathrm{s})\} \neq \{0, 0\}$ for all $m = 1, \ldots, n$. The inverse then has the form

$$\mathbf{A}^{-1}(k) = \mathbf{A}_1(k - k_\mathrm{s})^{-1} + \mathbf{A}_0 + \ldots \tag{C.1}$$

If $\mathbf{A}_{-1} \neq \mathbf{0}$ then $\mathbf{A}$ has zero eigenvalues.

References

[1] R. E. Collin. *Field Theory of Guided Waves*. IEEE Press, New York, second edition, 1991.

[2] G. H. Golub and C. F. van Loan. *Matrix Computations*. The Johns Hopkins University Press, Baltimore, Maryland, 1983.

[3] A. Ishimaru. *Electromagnetic Wave Propagation, Radiation, and Scattering*. Prentice-Hall, Inc., Englewood Cliffs, New Jersey, 1991.

[4] R. Kress. *Linear Integral Equations*. Springer-Verlag, Berlin Heidelberg, 1989.

[5] G. Kristensson, S. Poulsen, and S. Rikte. Propagators and scattering of electromagnetic waves in planar bianisotropic slabs — an application to frequency selective structures. Technical Report LUTEDX/(TEAT-7099)/1–32/(2001), Lund Institute of Technology, Department of Electroscience, P.O. Box 118, S-221 00 Lund, Sweden, 2001.

[6] G. Kristensson, P. Waller, and A. Derneryd. Radiation efficiency and surface waves for patch antennas on inhomogeneous substrates. Technical Report LUTEDX/(TEAT-7100)/1–48/(2001), Lund Institute of Technology, Department of Electroscience, P.O. Box 118, S-221 00 Lund, Sweden, 2001. `http://www.es.lth.se`.

[7] S. Poulsen. Scattering from frequency selective surfaces: A continuity condition for entire domain basis functions and an improved set of basis functions for crossed dipole. *IEE Proc.-H Microwaves, Antennas and Propagation*, **146**(3), 234–240, 1999.

[8] D. M. Pozar and D. H. Schaubert. Scan blindness in infinite phased arrays of printed dipoles. *IEEE Trans. Antennas Propagat.*, **32**(6), 602–610, 1984.

[9] S. Rikte, G. Kristensson, and M. Andersson. Propagation in bianisotropic media—reflection and transmission. Technical Report LUTEDX/(TEAT-7067)/1–31/(1998), Lund Institute of Technology, Department of Electromagnetic Theory, P.O. Box 118, S-221 00 Lund, Sweden, 1998.

[10] S. Rikte, G. Kristensson, and M. Andersson. Propagation in bianisotropic media—reflection and transmission. *IEE Proc. Microwaves, Antennas and Propagation*, **148**(1), 29–36, 2001.

[11] W. Wasow. *Asymptotic Expansion for Ordinary Differential Equations*. Dover Publications, New York, 1965.